NASA
Technical
Paper
2661

May 1987

Modeling of Joints for the Dynamic Analysis of Truss Structures

W. Keith Belvin

NASA

NASA Technical Paper 2661

1987

Modeling of Joints for the Dynamic Analysis of Truss Structures

W. Keith Belvin

Langley Research Center
Hampton, Virginia

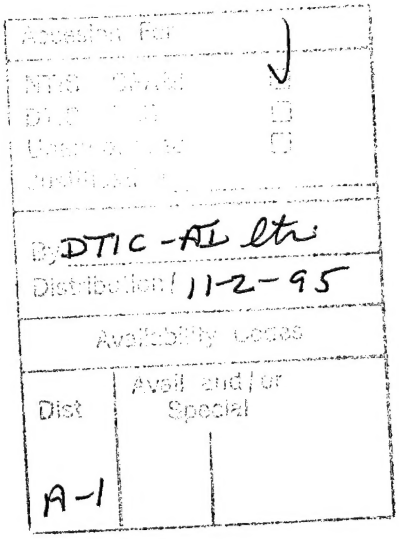

National Aeronautics and Space Administration

Scientific and Technical Information Branch

Summary

A method for modeling joints to assess the influence of joints on the dynamic response of truss structures has been developed. The analytical models, which are based on experimental joint load-deflection behavior, use springs and dampers to simulate joint behavior. An algorithm for automatically computing nonlinear coefficients of the analytical models is also presented. The joint models are incorporated into a nonlinear finite-element program through use of special nonlinear spring, viscous, and friction elements. Next, the effects of nonlinear joint stiffness, such as dead band in the joint load-deflection behavior, are studied. Linearization of joint stiffness nonlinearities is performed to assess the accuracy of linear analysis in predicting nonlinear response. Viscous and friction damping are then used to show the effects of joint damping on global beam and truss structure response and equations for predicting the sensitivity of beam deformations to changes in joint stiffness are derived. In addition, the frequency sensitivity of a truss structure to random perturbations in joint stiffness is discussed and results are shown which indicate that average joint properties may be sufficient for predicting truss response.

Introduction

The increased access to space made possible by the NASA Space Transportation System has resulted in radically new spacecraft designs. Spacecraft larger than 300 ft in diameter, such as the hoop-column antenna (ref. 1) and the Space Station reference configurations (ref. 2), are being designed. These spacecraft, shown in figures 1 and 2, make extensive use of truss structures to span large distances because trusses provide high stiffness with low mass. Many of these spacecraft require accurate dynamic analysis for prediction of loads, stability, shape control, and pointing accuracy. The dynamic analysis of truss structures may require detailed modeling to maintain accuracy in the analysis.

Individual truss members are connected to one another through joints. In most civil engineering truss structures, joints are typically welded or bolted so that little or no displacement occurs across the joint relative to the displacement of the members. For this type of joint, analytical modeling assumes either member-to-member rigid or pinned connections. Truss structures proposed for space applications have joint designs which permit the erection or deployment of the truss members. Unlike civil engineering structures, joint designs for space structures have finite tolerances between mating surfaces which permit the joints to rotate or to be latched. Tolerances result in a region of dead band where joint motion can occur with near-zero force. Joint dead band is believed to significantly affect the response of truss structures and may require detailed modeling to include these effects in the overall, or global, analysis.

Truss structures are often referred to as being "joint dominated" because of the number of joints and their influence on overall truss response. The joints influence the dynamic response of trusses in two major ways, first by reducing the effective truss stiffness and second by introducing additional damping compared with structures for which the members are rigidly connected. To predict the influence of joints on truss response, detailed characterization of joint properties will likely be necessary. Several publications describe experimental characterizations of joints and modeling of jointed structures.

Built-up structures possess a number of mechanisms to dissipate energy resulting from the mechanical interfaces or joints which join structural components together. References 3 to 7 discuss a large number of joint tests and analyses to determine the dominant sources of joint damping. At low frequencies, there is uniform agreement that Coulomb friction mechanisms on a macroscopic level dissipate the majority of the energy. At higher frequencies, Aubert et al. (ref. 7) have identified a number of rate-dependent damping mechanisms that dissipate energy. Examples of rate-dependent joint damping mechanisms are acoustic radiation, air pumping, viscous damping, and impacting of surfaces. Only structures with low-frequency oscillations are considered in this study; thus, only Coulomb friction and viscous damping have been included in the analysis herein.

To obtain analytical models of joints, the damping and the stiffness of the joints should be measured from the joint hardware. Reference 8 has used classic load-deflection testing to measure joint stiffness. Load-deflection testing can also be used to extract damping information by testing at several different loading rates. At high frequencies, the individual load-deflection curves do not describe rate-dependent damping mechanisms adequately. Consequently, the authors of references 7 and 9 have used a modified load-deflection technique called force-state mapping. Force-state maps, as shown in figure 3, are produced from a three-dimensional plot of the joint response in which force, velocity, and displacement are displayed. Results from references 7 and 9 indicate force-state mapping is a viable joint test method even at relatively high frequencies. The joint test method used in this study is load-deflection testing. This method was chosen because only low-frequency vibrations are considered.

The majority of existing methods for modeling structures with joints use variations of the component synthesis method. Craig presents a good review of state-of-the-art synthesis methods in reference 10. For rigid connections, the basic methods presented in references 11 to 15 may be employed. However, when the connections are flexible, as is the case in practice, the number of viable component synthesis methods is reduced. One method which enables components to be connected through flexible joints is referred to as a stiffness coupling procedure (ref. 16). The stiffness coupling procedure allows natural vibration modes of components to be combined through a linear stiffness matrix. Another method has been proposed (refs. 17 to 20) which exploits Lagrange's equations and Lagrange multipliers to allow components to be connected through nonrigid constraint relations. In reference 20, a generalization of the Lagrange multiplier method permits the analysis of structures connected by nonlinear joints. For structures with only a few joints, this method is feasible. However, for structures with many joints, the Lagrange multiplier method requires the solution of many additional equations. Thus, component synthesis methods for systems with many nonlinear joints do not appear to be any more efficient than finite-element analysis methods. Consequently, the present study focuses on developing a finite-element-based analysis for detailed joint modeling because of its generality and ease of implementation.

The objective of this study is to develop a systematic procedure whereby the influence of joints on the response of truss structures can be quantitatively determined. This procedure can be broken into three areas. First, joint characteristics are determined experimentally. Second, analyses are developed which enable joint-dominated structure response to be accurately predicted. Third, numerical studies are made of the structure response. Several joint models are developed, and model stiffness and damping parameters are determined with an algorithm based on optimization techniques. Incorporation of the joint models into global structural analysis is performed with the finite-element method. Numerical examples of the transient response of beam and truss structures with joints are then presented. The effects of stiffness nonlinearities and viscous and frictional damping mechanisms are also studied. Finally, numerical results of linearized joint models are compared with full nonlinear results, and the sensitivity of global structure response to variations in joint properties is presented.

Nomenclature

A	cross-sectional area of the beam
$\mathbf{B}$	viscous damping matrix
C	magnitude of joint dead band
C_I	initial joint dead band position
c	viscous damping coefficient
E	Young's modulus of the beam material
E_d	energy dissipated by damping

$\mathbf{F}$	force vector
F^f	friction damping force
f	frequency
G	shear modulus of the beam material
I	moment of inertia of the beam cross section
$\mathbf{K}$	stiffness matrix
k	spring stiffness of the joint
k_u, k_w, k_ϕ	spring stiffness of the joints in the axial, lateral, and rotational displacement directions
$\tilde{k}_u, \tilde{k}_w, \tilde{k}_\phi$	normalized spring stiffness of the joints in the axial, lateral, and rotational displacement directions (see eqs. (10))
ℓ	total beam length
$\mathbf{M}$	mass matrix
m	nodal mass
$\mathbf{N}$	vector of friction forces
N_s	number of time steps
O	objective function
t	time
u	axial displacement
w	lateral displacement
X	total joint displacement
ρ	mass density of the beam material
ϕ	rotational displacement
$\boldsymbol{\psi}$	nodal displacement vector
$\dot{\boldsymbol{\psi}}$	nodal velocity vector
$\ddot{\boldsymbol{\psi}}$	nodal acceleration vector
ω	circular frequency
ω_{ss}	circular frequency of simply supported beam
Superscripts:	
a, b, c	parts of the joint model (see fig. 6)
Subscripts:	
a, b, c, d	nodes of the joint elements and of the beam
J	beam deformations with joints
R	beam deformations without joints

Analysis

Analytical joint models should permit joint damping and stiffness behavior to be simulated, but should be simple enough so that the model parameters can be identified from test data. The design

of truss structure joints can produce eccentricities in the load transmission path which result in coupling of axial, bending, torsion, and shear deformations. Thus, complete characterization of joint damping and stiffness requires a series of tests which can identify coefficients of fully populated damping and stiffness matrices. This task is even further complicated by the fact that many of the joint properties are nonlinear, so that linear superposition cannot be used. Assumptions in the analysis are required to permit the model parameters to be identified through a limited series of tests. The present study uses a nonlinear model for the load-deflection relationship; however, coupling between axial, bending, torsion, and shear deflections has been neglected. This simplifying assumption results in identification of only the diagonal terms of the joint damping and stiffness matrices.

The joint model development method used herein follows the flowchart of figure 4. Three major components of model development are involved. First, choose the form of the joint analysis model to be used in the global analysis of the truss structure. Second, design and conduct a series of experiments to determine the load-deflection behavior of the joint. The type of experiment depends on the form of the chosen analysis model. For example, if no rate-dependent damping is modeled in the analysis, only static tests are required. Third, determine coefficients of the analytical model which most closely reconstruct the experimental joint behavior. This is usually accomplished through minimization of the error between the predicted and the measured response.

The next three sections discuss the three components of joint model development. An extension of the standard anelastic model (ref. 19) is described, followed by a description of experimental tests which can be used to characterize joint behavior. Sample experimental data are presented from a representative space truss joint, and an algorithm is used to reduce the experimental data into coefficients of the joint analytical model. Numerical results from the algorithm are presented for both simulated and experimental data. Subsequently, the finite-element program for global analysis of beam and truss structures is described.

Model Selection

Analytical models for truss structure joints should be of a form which can be incorporated into the global structure analysis. This study uses the finite-element method for the global analysis; thus, it is only natural that the joint models should be finite elements. Linear springs and linear viscous dampers are the simplest joint finite elements. As described previously, a number of nonlinear stiffness and damping mechanisms are present in structural joints. Consequently, nonlinear springs and dampers have been chosen to model the joint response.

In reference 21, Lazan presented several models which have been used in material stiffness and damping analysis. The Maxwell model consists of a viscous damper in series with a spring. The Maxwell model, shown in figure 5, exhibits infinite creep as the frequency of excitation approaches zero. The Voight model eliminates the creep problem by placing the spring in parallel with the damper. Unfortunately, the Voight model becomes rigid at high frequencies. An anelastic model of a Voight unit in series with a spring is also shown in figure 5. This three-parameter model, referred to as the standard anelastic model, exhibits none of the limitations of the Voight or Maxwell models.

Since joints exhibit material damping characteristics as well as macroscopic Coulomb friction, the standard anelastic model has been modified as shown in figure 5. The standard anelastic model is augmented with a friction-spring unit placed in series with the other elements. The resulting model is referred to herein as the modified standard anelastic (MSA) model. Nonlinear response of the MSA model can be achieved if some or all of the coefficients are allowed to be functions of displacement, velocity, or load, or any combination of these three. Displacement-dependent coefficients have been used in this study for the stiffness, friction, and viscous coefficients.

The MSA model has four nodes, as indicated in figure 6. For each degree of freedom (DOF) a different set of coefficients relates the displacement of that degree of freedom to the applied load.

The MSA model has three components in series, and the total displacement across the joint is

$$(\psi_a - \psi_d) = (\psi_a - \psi_b) + (\psi_b - \psi_c) + (\psi_c - \psi_d) \tag{1}$$

where ψ is the nodal displacement vector. For the planar structures analyzed in this study, three degrees of freedom at each node are present and

$$\psi = \begin{Bmatrix} u \\ w \\ \phi \end{Bmatrix}$$

For a force $\mathbf{F}_\psi$ applied to the joint model, the displacement across the viscous unit is given by

$$\mathbf{M}_\psi \ddot{\psi} + \mathbf{B}_\psi \dot{\psi} + \mathbf{K}_\psi \psi + \mathbf{N}_\psi = \mathbf{F}_\psi \tag{2}$$

where

$$\mathbf{M}_\psi = \begin{bmatrix} m_a & 0 & 0 & 0 \\ 0 & m_b & 0 & 0 \\ 0 & 0 & m_c & 0 \\ 0 & 0 & 0 & m_d \end{bmatrix}$$

$$\mathbf{B}_\psi = \begin{bmatrix} c & -c & 0 & 0 \\ -c & c & 0 & 0 \\ 0 & 0 & 0 & 0 \\ 0 & 0 & 0 & 0 \end{bmatrix}$$

$$\mathbf{K}_\psi = \begin{bmatrix} k^a & -k^a & 0 & 0 \\ -k^a & k^a + k^b & -k^b & 0 \\ 0 & -k^b & k^b + k^c & -k^c \\ 0 & 0 & -k^c & k^c \end{bmatrix}$$

$$\mathbf{N}_\psi = \begin{Bmatrix} 0 \\ F^f \operatorname{sgn}\left(\dot{\psi}_b - \dot{\psi}_c\right) \\ -F^f \operatorname{sgn}\left(\dot{\psi}_b \dot{\psi}_c\right) \\ 0 \end{Bmatrix}$$

$$\mathbf{F}_\psi = \begin{Bmatrix} F \\ 0 \\ 0 \\ -F \end{Bmatrix}$$

The modified standard anelastic model with constant coefficients (i.e., k^a_ψ, k^b_ψ, k^c_ψ, c_ψ, and F^f_ψ) results in linear load-deflection relations (with the exception of friction). To allow for more general nonlinear load-deflection relations, a polynomial function for each coefficient can be used. Figure 7 shows the load-deflection shape functions for constant coefficients and variable coefficients. The sum

of these shape functions describes the total joint displacement. The variable coefficients used in this study to permit nonlinear force displacement behavior are

$$\left.\begin{aligned} k^a &= \sum_{r=1}^{s} k^a_{r\psi} \left(\psi_a - \psi_b\right)^{r-1} \\ k^b &= \sum_{r=1}^{t} k^b_{r\psi} \left(\psi_b - \psi_c\right)^{r-1} \\ k^c &= \sum_{r=1}^{u} k^c_{r\psi} \left(\psi_c - \psi_d\right)^{r-1} \\ F^f &= \sum_{r=1}^{v} F^f_{r\psi} \left(\psi_b - \psi_c\right)^{r-1} \\ c &= \sum_{r=1}^{w} c_{r\psi} \left(\psi_a - \psi_b\right)^{r-1} \end{aligned}\right\} \tag{3}$$

where s, t, u, v, and w are the number of terms in the polynomial and subscript r refers to the rth coefficient of the polynomial.

The modified standard anelastic model with variable coefficients allows general nonlinear behavior to be modeled. However, the polynomial expressions used for the stiffness coefficients do not adequately account for changes in load-deflection behavior because of joint dead band. Figure 8 shows a load-deflection response in the presence of dead band C and with initial joint dead band position C_I. To model the dead band, the stiffness of each spring is modeled in a piecewise manner, such that

$$\left.\begin{aligned} k &= 0 && \left(-\frac{C}{2} - C_I \le \psi_a - \psi_b \le \frac{C}{2} - C_I\right) \\ k &= \sum_{r=1}^{n} k_{r\psi} \left(\psi_a - \psi_b - \frac{C}{2} + C_I\right)^{r-1} && \left(\psi_a - \psi_b > \frac{C}{2} - C_I\right) \\ k &= \sum_{r=1}^{n} k_{r\psi} \left(\psi_a - \psi_b + \frac{C}{2} + C_I\right)^{r-1} && \left(\psi_a - \psi_b < -\frac{C}{2} - C_I\right) \end{aligned}\right\} \tag{4}$$

where n is the number of terms in the polynomial representing the spring element amplitude-dependent stiffness behavior. Equation (4) is a general expression for nonlinear stiffness, including a region of zero stiffness (or dead band).

The modified standard anelastic model permits arbitrary damping and stiffness nonlinearities by allowing independent stiffness, friction, and viscous mechanisms to occur. This allows general load-deflection behavior, but it requires the use of four nodes in the analysis model. Since the joint analysis model is to be incorporated into a global analysis, a joint model with fewer nodes is desired to minimize the number of equations in the analysis. A second model with only two nodes that uses a spring, a viscous damper, and a friction damper in parallel could be constructed as shown in figure 9. With the nomenclature of figure 9, the displacement across the joint is given by equation (2)

$$\mathbf{M}_\psi \ddot{\boldsymbol{\psi}} + \mathbf{B}_\psi \dot{\boldsymbol{\psi}} + \mathbf{K}_\psi \boldsymbol{\psi} + \mathbf{N}_\psi = \mathbf{F}_\psi$$

where

$$\left.\begin{aligned}
\mathbf{M}_{\psi} &= \begin{bmatrix} m_a & 0 \\ 0 & m_b \end{bmatrix} \\
\mathbf{B}_{\psi} &= \begin{bmatrix} c & -c \\ -c & c \end{bmatrix} \\
\mathbf{K}_{\psi} &= \begin{bmatrix} k & -k \\ -k & k \end{bmatrix} \\
\mathbf{N}_{\psi} &= \begin{Bmatrix} F^f \operatorname{sgn}\left(\dot{\psi}_a - \dot{\psi}_b\right) \\ -F^f \operatorname{sgn}\left(\dot{\psi}_a - \dot{\psi}_b\right) \end{Bmatrix} \\
\mathbf{F}_{\psi} &= \begin{Bmatrix} F \\ -F \end{Bmatrix}
\end{aligned}\right\} \tag{5}$$

Nonlinear motion can be modeled with variable coefficients of the form given in equations (3) and (4). We can construct a fully linearized two-node model by setting $F_{\psi}^{f} = 0$ and using constant coefficients for c_{ψ} and k_{ψ}. A two-node linear representation of stiffness and damping is the simplest model for a joint. The modified standard anelastic model, the nonlinear two-node model, and the linear two-node model are summarized in figure 10.

Several observations can be made about the MSA model. The displacement of a joint for this model is both force and rate dependent. The rate dependence results from the viscous unit. Although the modified standard anelastic model requires more than two nodes, the additional insight provided by independent stiffness, viscous, and friction mechanisms can be useful. The nonlinear two-node model is the simplest nonlinear model to include in a global analysis. The two major limitations of this model are rigidity at high frequencies and coupled friction, viscous, and stiffness mechanisms. The first limitation results from the viscous damper being in parallel with the spring. This limitation is acceptable for low-frequency vibrations. The second limitation prevents independent friction, viscous, and stiffness mechanisms from occurring. Nevertheless, this model will be used often in global structural analysis because it requires only two nodes. The linear two-node model is the simplest model one can use to model both stiffness and damping effects of joints. Because the model is linear, almost all finite-element programs can use this model in a global structural analysis. In addition, it is advantageous to have a linear representation of structures for load analyses and control system design.

Load-Deflection Tests

Characterization of joint damping and stiffness properties requires both static and dynamic testing. Accurate measurement of load-deflection behavior requires precise instrumentation and experimental setups. Test data for this study have been acquired with the Instron Model 1350 Dynamic Test System and the MTS Systems Corp. closed-loop materials test system for load-deflection testing. General capabilities of Instron and MTS machines include force or displacement control, internal load and displacement measuring devices, and programmable force or displacement time histories. For joints where dead band is expected, displacement control is desirable because the force cannot be servo controlled with zero stiffness. Classic load-deflection hysteresis loops are measured under either sinusoidally controlled applied displacement or load. The circular frequency ω can be used to change the rate of applied displacement or load.

Tests should be performed at near-zero frequency (quasi-static) and at several higher frequencies. The quasi-static tests permit rate-independent stiffness and friction measurements without the complication of rate-dependent damping. Tests at selected higher frequencies can be used to determine rate-dependent mechanisms such as viscous and impact damping. Reference 7 presents an excellent discussion on instrumentation requirements and data acquisition systems and should be studied before joint testing is undertaken. As mentioned previously, the load-deflection testing

technique presented herein is mainly applicable at low frequencies, where the rate-dependent damping mechanisms are not dominant.

Joints for truss structures are of many different designs. Two typical joints are shown in figure 11. A joint of the design shown in figure 11(b) has been tested with the load-deflection procedure for the axial degree of freedom. Test data measured at a frequency of 1 Hz are shown in figure 12. The nonlinear character of the response is indicated by the joint stiffening or hardening as the displacement increases. Also, the stiffness in compression is different from that in tension. The pointed ends of the hysteresis loop indicate the presence of friction. These data were obtained at higher stress levels than are anticipated for space structures to show the nature of joint nonlinearities. For this joint the dead band is negligible. The next section describes an algorithm to reduce the data of figure 12 into coefficients of the joint analysis models described earlier.

Curve-Fit Algorithm

The least-squares error method is commonly used to identify coefficients of analytical models from test data. This method minimizes the error between measured and predicted response quantities. Classic least-squares error minimization is applicable only to linear systems. Since the joint models have nonlinear equations, a modified least-squares error method was developed based on optimization strategy. Numerical results of the algorithm for simulated and experimental data follow.

The coefficients of equation (2), which describes the displacement of the MSA model for applied force vector $\mathbf{F}_\psi$, can be determined by a trial-and-error procedure through use of an optimization procedure. The ADS program (ref. 22) is a compilation of optimization procedures which perform constrained and unconstrained minimizations. This program has been used as a subroutine for an algorithm developed specifically for joint damping and stiffness analysis. The algorithm requires an analytical joint model and experimental load-deflection joint data as input. Output from the algorithm are analysis model coefficients and the mean-squared error between the experimental data and the analysis prediction.

An unconstrained objective function is used in the algorithm, which minimizes the mean-squared error between test and analysis by minimizing the function

$$O = \frac{1}{N_s} \sum_{g=1}^{N_s} (X_{eg} - X_{ag})^2 \tag{6}$$

where N_s is the number of time steps, X is the total joint displacement, and subscripts e and a refer to experiment and analysis, respectively. Equation (6) is minimized through adjustment of the design variables, which are the coefficients of equation (2). Since the objective function O is unconstrained, the Davidon-Fletcher-Powell variable metric method is used in conjunction with a golden section search method. Both methods are contained in the ADS program.

In an optimization procedure, a solution strategy must be devised to ensure convergence. This is particularly important when the design variables have significantly different effects on the objective function. Design variables of the joint models are selected to be stiffness and damping coefficients. The stiffness design variables govern the slope of the load-deflection curve, whereas the damping design variables govern the area enclosed by the curve. From trial and error, a three-pass solution strategy was developed to obtain a converged solution in the curve-fit algorithm.

The flowchart of figure 13 shows the three-pass solution strategy of the algorithm. Pass 1 is made with only stiffness coefficients to obtain the proper slope of the load-deflection curve. The damping coefficients are set to zero. Pass 2 sets the stiffness coefficients to the values obtained from pass 1 and allows the damping coefficients to be varied. Pass 2 usually produces a good estimate of the damping; however, a third pass reduces the objective function further. Pass 3, the third and final pass in the solution, uses the stiffness and damping coefficients from passes 1 and 2 as starting values. With all coefficients free to be varied, the final solution is achieved.

Variable stiffness and damping coefficients of the form given in equation (3) are solved in a manner analogous to that described for constant coefficients. The number of design variables is equal to the total number of unknown coefficients. For the general nonlinear modified standard anelastic model, stiffness, dead band, friction, and viscous coefficients are present.

The polynomial form used to model nonlinearities can produce local minima of the objective function. Optimization methods often converge to one of the local minima when the starting values of the design variables are not close to the true minimum. Thus, good estimates of the stiffness and damping coefficients are necessary. The algorithm has a preprocessor which estimates the stiffness coefficients based on the initial slope of the empirical data. The damping coefficients are estimated in the preprocessor through computation of the energy dissipated per cycle in the experimental data. The energy dissipation is initially divided equally between the friction and viscous damping mechanisms.

Simulated and experimental data have been curve fit with the algorithm. Figure 14 shows the load-deflection response of the modified standard anelastic model with constant coefficients. The dashed curve is simulated data computed with the following values:

$$
\begin{aligned}
k_{\psi}^{a} &= 400 \text{ lb/in.} \\
k_{\psi}^{b} &= 600 \text{ lb/in.} \\
k_{\psi}^{c} &= 800 \text{ lb/in.} \\
F_{\psi}^{f} &= 10 \text{ lb} \\
c_{\psi} &= 2.5 \text{ lb-sec/in.} \\
\mathbf{F}_{\psi} &= 100 \ \sin 2\pi t \text{ lb}
\end{aligned}
$$

The joint mass has been divided equally at each node with a total joint weight of 1 lb in the simulated data. The simulated data were analyzed with the algorithm, which computed the following coefficients:

$$
\begin{aligned}
k_{\psi}^{a} &= 572 \text{ lb/in.} \\
k_{\psi}^{b} &= 511 \text{ lb/in.} \\
k_{\psi}^{c} &= 569 \text{ lb/in.} \\
F_{\psi}^{f} &= 11.7 \text{ lb} \\
c_{\psi} &= 1.16 \text{ lb-sec/in.}
\end{aligned}
$$

A comparison of the simulated and the predicted load-deflection curves in figure 14 shows very good agreement. The simulated coefficient values and the predicted coefficient values, however, are considerably different. The total response is accurate since it is the combination of coefficients which is important and not the individual coefficients. That is, with three springs in series in the modified standard anelastic model there is no unique solution for the stiffness coefficients. Thus, the algorithm converges to one of the local minima close to the true minimum.

To study the effects of nonlinearities, simulated nonlinear data were analyzed with the algorithm. The simulated data maintained constant damping coefficients, but the stiffness coefficients were variable. The coefficient values are

$$
\left.
\begin{aligned}
k_{\psi}^{a} &= 400 + 600|\psi_a - \psi_b| + 8000\,(\psi_a - \psi_b)^2 \text{ lb/in.} \\
k_{\psi}^{b} &= 400 + 600|\psi_b - \psi_c| + 8000\,(\psi_b - \psi_c)^2 \text{ lb/in.} \\
k_{\psi}^{c} &= 400 + 600|\psi_c - \psi_d| + 8000\,(\psi_c - \psi_d)^2 \text{ lb/in.} \\
F_{\psi}^{f} &= 15 \text{ lb} \\
c_{\psi} &= 20 \text{ lb-sec/in.}
\end{aligned}
\right\} \tag{7}
$$

The absolute value of the displacement was used to obtain symmetric tension and compression response. The simulated nonlinear data were analyzed with two analysis models. First, the MSA model with constant coefficients was used. The response, as shown in figure 15, did not match the simulated data accurately. The constant coefficients computed with the algorithm are

$$
\begin{aligned}
k_{\psi}^{a} &= 667.6 \text{ lb/in.} \\
k_{\psi}^{b} &= 466.4 \text{ lb/in.} \\
k_{\psi}^{c} &= 656.2 \text{ lb/in.} \\
F_{\psi}^{f} &= 28.5 \text{ lb} \\
c_{\psi} &= 2.6 \text{ lb-sec/in.}
\end{aligned}
$$

The second model used to predict the simulated nonlinear data given by equation (7) used the MSA model with constant damping coefficients but variable stiffness coefficients of the following form:

$$
\left.
\begin{aligned}
k_{\psi}^{a} &= k_{1\psi}^{a} + k_{2\psi}^{a}|\psi_a - \psi_b| + k_{3\psi}^{a}(\psi_a - \psi_b)^2 \\
k_{\psi}^{b} &= k_{1\psi}^{b} + k_{2\psi}^{b}|\psi_b - \psi_c| + k_{3\psi}^{b}(\psi_b - \psi_c)^2 \\
k_{\psi}^{c} &= k_{1\psi}^{c} + k_{2\psi}^{c}|\psi_c - \psi_d| + k_{3\psi}^{c}(\psi_c - \psi_d)^2
\end{aligned}
\right\} \tag{8}
$$

The response from use of this model agreed well with the simulated data, as shown in figure 16. The coefficients computed with the algorithm are

$$
\begin{aligned}
k_{\psi}^{a} &= 462 + 1119|\psi_a - \psi_b| + 3215(\psi_a - \psi_b)^2 \text{ lb/in.} \\
k_{\psi}^{b} &= 424 + 1108|\psi_b - \psi_c| + 3202(\psi_b - \psi_c)^2 \text{ lb/in.} \\
k_{\psi}^{c} &= 375 + 1100|\psi_c - \psi_d| + 3228(\psi_c - \psi_d)^2 \text{ lb/in.} \\
F_{\psi}^{f} &= 6.8 \text{ lb} \\
c_{\psi} &= 12 \text{ lb-sec/in.}
\end{aligned}
$$

Even though the simulated data were produced by the same model used in the analysis, exact agreement was not obtained. This is because of the presence of local minima to which the optimization algorithm converged. Should the algorithm converge to a local minimum of unacceptable accuracy, the solution should be restarted with different estimates for the design variables.

The algorithm was also used to analyze the test data of figure 12. The test data were modified to preserve tension and compression symmetry. The data were analyzed with the modified standard anelastic (MSA) model with constant damping coefficients and variable stiffness coefficients of the form given in equation (8). The predicted load-deflection curve is compared with the test data in figure 17. Again the curve fit is good. The coefficients for these data computed with the algorithm are

$$
\begin{aligned}
k_{\psi}^{a} &= 31\,264 + (4.943 \times 10^{6})|\psi_a - \psi_b| + (1.775 \times 10^{8})(\psi_a - \psi_b)^2 \text{ lb/in.} \\
k_{\psi}^{b} &= 28\,074 + (3.735 \times 10^{6})|\psi_b - \psi_c| + (1.528 \times 10^{8})(\psi_b - \psi_c)^2 \text{ lb/in.} \\
k_{\psi}^{c} &= 26\,696 + (4.145 \times 10^{6})|\psi_c - \psi_d| + (1.693 \times 10^{8})(\psi_c - \psi_d)^2 \text{ lb/in.} \\
F_{\psi}^{f} &= 229.7 \text{ lb} \\
c_{\psi} &= 96 \text{ lb-sec/in.}
\end{aligned}
$$

The ability of the algorithm to reduce experimental data into a set of stiffness and damping coefficients for empirical joint models has been shown. The joint analytical model parameters identified with the curve-fit algorithm can be included in a global truss structure analysis through use of the finite-element method. The next section describes the global analysis used in this study.

Global Structure Analysis

A mixed finite-element program for beams and two-dimensional trusses (refs. 23 and 24) has been modified to include nonlinear joint properties. An analytical formulation by Reissner (ref. 25) for geometrically nonlinear curved beams forms the basis of this program. The program has been used because of its availability and ease of modification for inclusion of nonlinear joint elements. Several modifications to the program were made to permit modeling of joints, damping, and truss configurations.

The fundamental unknowns of the mixed program are nodal forces, velocities, and displacements. Four types of elements have been formulated for use in a finite-element model: beams, springs, viscous dampers, and friction dampers. A consistent formulation for each type of element has been used to maintain compatibility with the field variables. The beam element formulation is described in reference 23; thus, only the joint elements are described herein.

A one-dimensional spring element with two displacement nodes and one stress node has been formulated. A typical two-dimensional joint requires three spring elements to represent the joint load-deflection behavior, one element for each degree of freedom. Nonlinear load-deflection response of a joint is modeled with displacement-dependent stiffness parameters. The spring element governing equations are derived with an energy formulation. Figure 18 shows a typical spring element with lumped masses and external loads at the two displacement nodes a and b. With the sign convention shown, the constitutive relation for the spring element is defined as

$$\mathbf{F} = \sum_{r=1}^{n} \left[k_{r\psi} \left(\psi_a - \psi_b \right)^r \right]$$

where $\mathbf{F}$ is the internal spring force vector, $k_{1\psi}$ is the linear stiffness of the spring for the ψth degree of freedom, $k_{r\psi}$ $(r > 1)$ are nonlinear stiffness coefficients, and n is the number of terms in the polynomial representing the spring element amplitude-dependent stiffness behavior. (For a linear spring element, $n = 1$.)

The polynomial form of the constitutive relations permits modeling of continuous nonlinear load-deflection behavior. However, joint load-deflection response can exhibit a region of dead band where essentially no force is required to produce a relative displacement between the joint ends. This dead band can be modeled in a piecewise manner. Figure 8 shows load-deflection response in the presence of dead band C. In addition, the initial position of the joint is described by the quantity C_I. The force transmission of the joint is

$$\left.\begin{aligned}
\mathbf{F} &= 0 && \left(-\frac{C}{2} - C_I \le \psi_a - \psi_b \le \frac{C}{2} - C_I \right) \\
\mathbf{F} &= \sum_{r=1}^{n} k_{r\psi} \left(\psi_a - \psi_b - \frac{C}{2} + C_I \right)^r && \left(\psi_a - \psi_b > \frac{C}{2} - C_I \right) \\
\mathbf{F} &= \sum_{r=1}^{n} k_{r\psi} \left(\psi_a - \psi_b + \frac{C}{2} + C_I \right)^r && \left(\psi_a - \psi_b < -\frac{C}{2} - C_I \right)
\end{aligned}\right\} \tag{9}$$

For generality, equation (9) has been used in the spring element formulation.

A one-dimensional viscous damper element similar to the spring element formulation has been formulated to permit modeling of viscous damping mechanisms. Nonlinear viscous damping has been modeled with displacement-dependent viscous parameters.

The following energy dissipation term E_d has been added to the total energy functional:

$$E_d = \sum_{r=1}^{n} c_{r\psi} \left(\dot{\psi}_a - \dot{\psi}_b \right) (\psi_a - \psi_b)^r$$

This energy dissipation term reduces to classic linear rate-dependent viscous damping for $n = 1$. For $n > 1$, nonlinear damping is modeled as being dependent on both velocity and displacement. This allows general treatment of nonlinear rate-dependent damping mechanisms.

A one-dimensional friction element has been formulated to permit modeling of frictional damping mechanisms. The energy dissipation term is defined as

$$E_d = \sum_{r=1}^{n} F^f_{r\psi} (\psi_a - \psi_b)^r \left[\text{sgn} \left(\dot{\psi}_a - \dot{\psi}_b \right) \right]$$

This energy dissipation term reduces to classic Coulomb friction for $n = 1$. For $n > 1$, amplitude-dependent friction can be modeled.

The governing equations for the entire structure are obtained from assembly of the elemental contributions. The structure governing equations given can be integrated in time to solve for the time history response of the structure. An explicit half-station central-difference integration technique has been used in this study. The disadvantage of explicit integration is the small time-step size required for numerical stability. The finite-element analysis program as it currently exists can solve for structures with up to 150 degrees of freedom using approximately 200 kilobytes of core memory. The next section presents numerical results of the finite-element program for several beam and truss structures with linear and nonlinear joints.

Results and Discussion

This section presents numerical solutions from the finite-element program to study the effects of joints on transient response of beam and truss structures. In addition, eigenvalue analysis has been performed to study the sensitivity of the fundamental vibration frequency to changes in linear joint stiffness.

A beam with joints at each end has been analyzed to study the behavior of individual truss members. The beam was loaded with a step load such that the frequency and amplitude of vibration could be determined from the transient response. Changes in global beam response because of changes in joint stiffness characteristics have been investigated and beam response with nonlinear joint stiffness has been compared with that with linearized joint stiffness. Viscous and friction damping in the joints have been modeled to evaluate global beam damping.

Also, the transient response of a planar, cantilevered, four-bay truss subjected to a tip step load has been modeled to study global truss response. The truss response with nonlinear joint stiffness and with linearized joint stiffness is presented. Damping of global truss response resulting from friction damping in the joints is also shown.

In addition, the sensitivity of beam deformations to changes in linear joint stiffness has been analyzed. Expressions for beam response with joints have been used to compute sensitivity derivatives of beam response to changes in joint stiffness. The sensitivity of the fundamental truss frequency has been numerically evaluated by random perturbations in joint stiffness in each of the truss structure joints. Thirty-five cases have been analyzed to obtain a limited statistical basis for predicting the sensitivity of structural response to perturbations in linear joint stiffness.

Beam Response

In order to assess the behavior of individual truss members, a beam with joints at each end (shown in fig. 19) has been studied. The beam has homogeneous properties; however, joints attach

the beam to the ground. The beam properties represent those of proposed Space Station truss members given in reference 2. The beam is a 2-in.-diameter tube with a 0.060-in. wall thickness and is 108 in. long. Graphite/epoxy materials with the following properties were used to construct the beam:

$$E = 40.7 \times 10^6 \text{ lb/in}^2$$

$$G = 7 \times 10^5 \text{ lb/in}^2$$

$$\rho = 1.132 \times 10^{-4} \text{ lb-sec}^2/\text{in}^4$$

For planar vibrations, three degrees of freedom have been permitted for each node. Each joint consists of three spring elements k_u, k_w, and k_ϕ, one in each degree of freedom. Linear joint stiffnesses have been normalized with the linear beam stiffness properties such that

$$\tilde{k}_u = \frac{k_u}{EA/\ell} \qquad \tilde{k}_w = \frac{k_w}{EI/\ell^3} \qquad \tilde{k}_\phi = \frac{k_\phi}{4EI/\ell} \tag{10}$$

Each joint has a lumped mass of 0.000826 lb-sec^2/in. and a rotational inertia of 0.000758 lb-in-sec^2.

Effect of joint stiffness on beam response. The rotational restraint provided by the joint can significantly alter the lateral vibration frequency of the beam shown in figure 19. Figure 20 shows the effect of joint rotational stiffness $\tilde{k}_\phi$ on the fundamental beam frequency. (The stiffnesses $\tilde{k}_u$ and $\tilde{k}_w$ have been set to large values to simulate rigid connections to ground in the axial and lateral directions.) For $\tilde{k}_\phi = 0$, the beam is simply supported ($\omega/\omega_{ss} = 1.0$). As the stiffness increases, the frequency of vibration asymptotically approaches the clamped-clamped frequency. This result is certainly well understood. However, the slope of the curve of figure 20 gives a great deal of insight into the importance of the rotational stiffness. For example, as $\tilde{k}_\phi$ approaches zero, further reductions in $\tilde{k}_\phi$ because of nonlinearities would have a very small effect. Similarly, as $\tilde{k}_\phi$ becomes very large, hardening nonlinearities would also produce little change. Thus, to study the effect of joint nonlinearities on beam response, it is reasonable to choose $\tilde{k}_\phi$ between 0.3 and 10.0.

To study nonlinear effects, the beam response to a step load (as indicated in fig. 19) has been calculated. The joint rotational stiffness has a hardening nonlinearity defined by

$$k_\phi = 5 \times 10^5 + 5 \times 10^{12} \left(\phi_{\text{joint}}\right)^2 \text{ in-lb}$$

where ϕ_{joint} is the rotational displacement of the joint. The response under a 10-lb load is shown in figure 21. For $\tilde{k}_\phi = 1.93 \left(k_\phi = 5 \times 10^5 \text{ in-lb}\right)$ the beam response is shown by the solid curve. The beam responds at predominantly one frequency ($f = 74.6$ Hz), although higher vibration modes have been excited, as shown by the slight change in amplitude from peak to peak. The beam response with nonlinear joint stiffness is shown by the dashed curve of figure 21. The response with hardening joint stiffness has a higher frequency ($f = 81.8$ Hz) and a decrease in amplitude compared with the response with linear joint stiffness. Nevertheless, the response is nearly sinusoidal, which indicates the possibility of linearization.

The nonlinear effect of dead band is shown in figure 22 for $k_\phi = 5 \times 10^5$ in-lb, $C = 0.001$ rad, and $C_I = 0$ rad. The dashed curve representing the nonlinear response shows a decrease in frequency ($f = 64.8$ Hz) and an increase in amplitude compared with the linear response. The response remains sinusoidal even with the joint dead band.

Since both hardening stiffness and dead band result in sinusoidal response, it appears that some form of linearization is possible. Figure 23 shows the beam response with joint stiffness linearized to match the frequency of the nonlinear beam response. Figure 23(a) shows the linearized response ($k_\phi = 6.7 \times 10^5$ in-lb) agrees with the nonlinear response in frequency, but the amplitude of vibration is smaller than the response with hardening joint stiffness. Similarly, figure 23(b) shows the linearized

response with $k_\phi = 2.4 \times 10^5$ in-lb agrees with the nonlinear response in frequency, but the amplitude is smaller than the response with the joint dead band. These results indicate that joint nonlinearities do result in true nonlinear global response; however, the frequency of vibration can be approximated with linear analysis for steady-state vibrations.

Effect of joint damping on beam response. Joint damping has been modeled with viscous and frictional elements in parallel with the rotational spring elements which represent the joint stiffness. Figure 24 shows the effect of joint viscous damping ($c_\phi = 300$ lb-in-sec/rad) on beam response under a 10-lb load. The dashed curve shows the response with the same dead band nonlinearity as used in figure 2. The vibration amplitude decays with time and approaches the static equilibrium value of displacement. The frequency of vibration also decreases with decreasing amplitude. The solid curve of figure 24 shows the response of a beam with $c_\phi = 300$ lb-in-sec/rad and with the linearized stiffness from figure 23(b). The linearized response predicts the time of the first peak; however, the remainder of the response differs considerably from the true nonlinear response because of the dead band and the variation of frequency with decaying amplitude. Figure 25 shows the response of a beam with frictional damping in the joints ($F^f = 20$ in-lb). The dashed curve shows the response of a beam with joint dead band and friction. The vibration amplitude and frequency both decrease with time. The solid curve shows the beam response with linearized joint stiffness and $F^f = 20$ in-lb. The responses differ in both amplitude and frequency. It is interesting to note that although the linearized response contains only friction damping, the decay rate is not linear. This nonlinear decay rate may be attributed to the nonproportional nature of friction damping when present only in joints.

To summarize, it appears nonlinear joint stiffness can have significant effects on beam response. For constant vibration amplitudes, such as for steady-state vibrations or for undamped step loading, the nonlinear stiffness can be linearized to simulate the frequency of beam vibration with nonlinear joints. However, when the peak vibration amplitudes change with time because of damping, the frequency of vibration does not remain constant and cannot be linearized.

Truss Response

A cantilevered, four-bay truss, shown in figure 26, has been studied. The truss consists of 16 beam elements with the same properties as those discussed in the *Beam Response* section. There are 32 joints in the truss, 1 at each end of every beam. Both eigenvalue and transient response analyses have been performed.

Effect of joint stiffness on truss response. The stiffness of truss structures is strongly influenced by the axial stiffness of the joints. Figure 27 shows the frequency of the lateral bending truss mode as the stiffness parameter $\tilde{k}_u$ is changed. (The stiffnesses $\tilde{k}_w$ and $\tilde{k}_\phi$ have been set to large values to simulate rigid connections in the lateral and rotational directions.) For $\tilde{k}_u = 0$, the truss frequency vanishes. As $\tilde{k}_u$ increases, the truss frequency increases asymptotically to 35.2 Hz. A value of $\tilde{k}_u = 0.726$ has been chosen to study the transient response of the truss.

The transient response of the truss with an external step load of 10 lb has been simulated. As shown in figure 26, the load is applied at the free end. Figure 28 shows the response at the point of loading. The solid curve is for a linear axial joint stiffness of $k_u = 1 \times 10^5$ lb/in. The response is dominated by one frequency, $f = 20.9$ Hz. Also shown in figure 28 is a dashed curve representing the response with dead band in the joints ($k_u = 1 \times 10^5$ lb/in., $C = 0.0015$ in., and $C_I = 0$ in.). The response with joint dead band occurs with a lower frequency ($f = 16.0$ Hz) and a much higher amplitude than the response with linear joint stiffness. Using a lower linearized stiffness of $k_u = 4.9 \times 10^4$ lb/in., which takes the dead band into account, one derives the solid curve in figure 29. Then, the frequencies of response of both the linearized and the nonlinear response agree, although a difference in amplitude exists. Thus, as was the case for the beam, the truss response frequency can be simulated with linearized analysis for steady-state vibration.

Effect of joint damping on truss response. To evaluate the effect of joint damping on the response of the truss, friction elements have been placed in parallel with each joint axial spring element. Figure 30 shows the response of the truss with $k_u = 1 \times 10^5$ lb/in., $C = 0.0015$ in., and $C_I = 0$ in. in each joint. The dashed curve shows the response of the truss without damping. The solid curve shows the response with $F^f = 15$ lb. As is the case for the beam, the frequency of the response with nonlinear joint stiffness changes with time as the amplitude decays.

The degree of frequency shift because of joint dead band is directly related to the amplitude of vibration. For large vibration amplitudes, the additional displacement because of joint dead band is small, and the total reduction in joint stiffness and structural frequency would be small. For small vibration amplitudes, joint dead band can add significantly to the total joint displacement whereby the effective joint stiffness is reduced. This effective reduction in joint stiffness may or may not have an appreciable effect on global structural response, depending on the sensitivity of the response to joint stiffness. The next section contains a discussion of the sensitivity of global beam response to changes in joint stiffness.

Sensitivity of Global Response to Variations in Joint Stiffness

A beam with joints on each end has been analyzed to determine the sensitivity of beam deformations to variations in joint stiffness. Expressions for beam displacements with and without joints are presented. These expressions enable the analyst to determine when the joint flexibility needs to be modeled. Derivatives of these expressions with respect to the joint stiffness also allow one to determine the importance of nonlinearities. A truss structure has also been studied to determine the effect of random perturbations of joint stiffness. The axial stiffnesses of 32 joints have been perturbed, and the fundamental frequency of the truss was computed for 35 different cases. The analysis of a beam with joints is presented first, followed by the truss-joint perturbation study.

Sensitivity of beam deformation to joint stiffness. Two beams shown in figure 31 have been used to determine the sensitivity of beam deformations. The first beam (fig. 31(a)) has two nodes, nodes a and d, with displacement and force vectors, represented by $\boldsymbol{\psi}_R$ and $\mathbf{F}_R$, as follows:

$$\boldsymbol{\psi}_R = \begin{Bmatrix} u_a \\ w_a \\ \phi_a \\ u_d \\ w_d \\ \phi_d \end{Bmatrix} \qquad \mathbf{F}_R = \begin{Bmatrix} P_a \\ Q_a \\ T_a \\ P_d \\ Q_d \\ T_d \end{Bmatrix}$$

where P, Q, and T are the corresponding forces for motions u, w, and ϕ. If node d is constrained to the ground and external forces are applied only at the free end (as would be the case for a cantilever beam), the displacement and force vectors become

$$\boldsymbol{\psi}_R = \begin{Bmatrix} \boldsymbol{\psi}_{Ra} \\ 0 \end{Bmatrix} \qquad \mathbf{F}_R = \begin{Bmatrix} \mathbf{F}_{Ra} \\ \mathbf{F}_{Rd} \end{Bmatrix}$$

The deformations of the cantilever beam can be computed with a linear beam stiffness matrix such that

$$\mathbf{F}_{Ra} = \mathbf{K}_{Ra} \boldsymbol{\psi}_{Ra} \tag{11}$$

where

$$\mathbf{K}_{Ra} = \begin{bmatrix} \frac{EA}{\ell} & 0 & 0 \\ 0 & \frac{12EI}{\ell^3} & \frac{6EI}{\ell^2} \\ 0 & \frac{6EI}{\ell^2} & \frac{4EI}{\ell} \end{bmatrix}$$

Equation (11) can be rewritten as

$$\boldsymbol{\psi}_{Ra} = \begin{bmatrix} \frac{\ell}{EA} & 0 & 0 \\ 0 & \frac{\ell^3}{3EI} & -\frac{\ell^2}{2EI} \\ 0 & -\frac{\ell^2}{2EI} & \frac{\ell}{EI} \end{bmatrix} \mathbf{F}_{Ra} \tag{12}$$

Equation (12) relates displacements of the free end of the beam to applied forces.

A similar expression for beam deformations can be obtained for a beam with two joints at each end, as shown in figure 31(b). This beam has four nodes, and the displacement and force vectors are

$$\boldsymbol{\psi}_J = \begin{Bmatrix} \boldsymbol{\psi}_{Ja} \\ \boldsymbol{\psi}_{Jb} \\ \boldsymbol{\psi}_{Jc} \\ \boldsymbol{\psi}_{Jd} \end{Bmatrix} \qquad \mathbf{F}_J = \begin{Bmatrix} \mathbf{F}_{Ja} \\ \mathbf{F}_{Jb} \\ \mathbf{F}_{Jc} \\ \mathbf{F}_{Jd} \end{Bmatrix}$$

If we define nodes a and d to be boundary nodes with displacement $\boldsymbol{\psi}_J^B$ and nodes b and c to be internal nodes with displacement $\boldsymbol{\psi}_J^I$, the internal nodes can be removed through static condensation. For

$$\boldsymbol{\psi}_J^B = \begin{Bmatrix} \boldsymbol{\psi}_{Ja} \\ \boldsymbol{\psi}_{Jd} \end{Bmatrix} \qquad \boldsymbol{\psi}_J^I = \begin{Bmatrix} \boldsymbol{\psi}_{Jb} \\ \boldsymbol{\psi}_{Jc} \end{Bmatrix} \qquad \mathbf{F}_J^B = \begin{Bmatrix} \mathbf{F}_{Ja} \\ \mathbf{F}_{Jd} \end{Bmatrix} \qquad \mathbf{F}_J^I = \begin{Bmatrix} \mathbf{F}_{Jb} \\ \mathbf{F}_{Jc} \end{Bmatrix} = \begin{Bmatrix} 0 \\ 0 \end{Bmatrix}$$

the beam deformations are computed by

$$\begin{Bmatrix} \mathbf{F}_J^B \\ \mathbf{F}_J^I \end{Bmatrix} = \begin{bmatrix} \mathbf{K}^{BB} & \mathbf{K}^{BI} \\ \mathbf{K}^{IB} & \mathbf{K}^{II} \end{bmatrix} \begin{Bmatrix} \boldsymbol{\psi}_J^B \\ \boldsymbol{\psi}_J^I \end{Bmatrix} \tag{13}$$

where

$$\mathbf{K}^{BB} = \begin{bmatrix} k_u & 0 & 0 & 0 & 0 & 0 \\ 0 & k_w & 0 & 0 & 0 & 0 \\ 0 & 0 & k_\phi & 0 & 0 & 0 \\ 0 & 0 & 0 & k_u & 0 & 0 \\ 0 & 0 & 0 & 0 & k_w & 0 \\ 0 & 0 & 0 & 0 & 0 & k_\phi \end{bmatrix}$$

$$\mathbf{K}^{IB} = \mathbf{K}^{BI} = \begin{bmatrix} -k_u & 0 & 0 & 0 & 0 & 0 \\ 0 & -k_w & 0 & 0 & 0 & 0 \\ 0 & 0 & -k_\phi & 0 & 0 & 0 \\ 0 & 0 & 0 & -k_u & 0 & 0 \\ 0 & 0 & 0 & 0 & -k_w & 0 \\ 0 & 0 & 0 & 0 & 0 & -k_\phi \end{bmatrix}$$

$$\mathbf{K}^{II} = \begin{bmatrix} \frac{EA}{\ell} + k_u & 0 & 0 & -\frac{EA}{\ell} & 0 & 0 \\ 0 & \frac{12EI}{\ell^3} + k_w & \frac{6EI}{\ell^2} & 0 & -\frac{12EI}{\ell^3} & \frac{6EI}{\ell^2} \\ 0 & \frac{6EI}{\ell^2} & \frac{4EI}{\ell} + k_\phi & 0 & -\frac{6EI}{\ell^2} & \frac{2EI}{\ell} \\ -\frac{EA}{\ell} & 0 & 0 & \frac{EA}{\ell} + k_u & 0 & 0 \\ 0 & -\frac{12EI}{\ell^3} & -\frac{6EI}{\ell^2} & 0 & \frac{12EI}{\ell^3} + k_w & -\frac{6EI}{\ell^2} \\ 0 & \frac{6EI}{\ell^2} & \frac{2EI}{\ell} & 0 & -\frac{6EI}{\ell^2} & \frac{4EI}{\ell} + k_\phi \end{bmatrix}$$

Equation (13) is obtained through use of a linear beam stiffness matrix and springs which represent the joints. To remove nodes b and c, equation (13) is rewritten as

$$\mathbf{F}_J^B = \left[\mathbf{K}^{BB} - \mathbf{K}^{BI}\left(\mathbf{K}^{II}\right)^{-1}\mathbf{K}^{IB}\right]\boldsymbol{\psi}_J^B$$

If node d is constrained to the ground and forces are applied only to node a,

$$\boldsymbol{\psi}_J^B = \begin{Bmatrix} \boldsymbol{\psi}_{Ja} \\ 0 \end{Bmatrix} \qquad \mathbf{F}_J^B = \begin{Bmatrix} \mathbf{F}_{Ja} \\ \mathbf{F}_{Jd} \end{Bmatrix}$$

The deformation of node a can be written as $\boldsymbol{\psi}_{Ja} = \mathbf{K}_{Ja}^{-1}\mathbf{F}_{Ja}$, or

$$\boldsymbol{\psi}_{Ja} = \begin{bmatrix} \frac{\ell\tilde{k}_u + 2\ell}{EA\tilde{k}_u} & 0 & 0 \\ 0 & \frac{\left(4\ell^3\tilde{k}_\phi + 3\ell^3\right)\tilde{k}_w + 2\ell^3\tilde{k}_\phi}{12EI\tilde{k}_w\tilde{k}_\phi} & -\frac{2\ell^2\tilde{k}_\phi + \ell^2}{4EI\tilde{k}_\phi} \\ 0 & -\frac{2\ell^2\tilde{k}_\phi + \ell^2}{4EI\tilde{k}_\phi} & \frac{2\ell\tilde{k}_\phi + \ell}{2EI\tilde{k}_\phi} \end{bmatrix} \mathbf{F}_{Ja} \tag{14}$$

where $\tilde{k}_u$, $\tilde{k}_w$, and $\tilde{k}_\phi$ are defined by equation (10).

Equations (12) and (14) can be used to determine the change in beam deformations when joints are present. If equal loads are applied to the beam without joints and to the beam with joints, $\mathbf{F}_{Ra} = \mathbf{F}_{Ja}$ and

$$\mathbf{K}_{Ra}\boldsymbol{\psi}_{Ra} = \mathbf{K}_{Ja}\boldsymbol{\psi}_{Ja}$$

Thus, the displacement amplification with joints is

$$\boldsymbol{\psi}_{Ja} = \mathbf{K}_{Ja}^{-1}\mathbf{K}_{Ra}\boldsymbol{\psi}_{Ra}$$

or

$$\boldsymbol{\psi}_{Ja} = \begin{bmatrix} 1 + \frac{2}{\tilde{k}_u} & 0 & 0 \\ 0 & 1 + \frac{2}{\tilde{k}_w} + \frac{3}{2\tilde{k}_\phi} & \frac{\ell}{\tilde{k}_w} + \frac{\ell}{2\tilde{k}_\phi} \\ 0 & 0 & 1 + \frac{1}{2\tilde{k}_\phi} \end{bmatrix} \boldsymbol{\psi}_{Ra} \tag{15}$$

For $\mathbf{F}_{Ja} = \mathbf{F}_{Ra}$, equation (15) may be used to assess the change in beam deformation when joints are present. Figure 32 shows the effect of joint stiffness on beam deformations. Figure 32(a) shows the change in axial displacement ratio as the joint axial stiffness $\tilde{k}_u$ is varied. As $\tilde{k}_u$ increases, the axial

displacement becomes asymptotic to the displacement of a beam without joints (i.e., $u_J/u_R = 1$). The sensitivity of the response to changes in axial joint stiffness is

$$\frac{\partial}{\partial \tilde{k}_u}\psi_{Ja} = \begin{bmatrix} -\frac{2}{\tilde{k}_u^2} & 0 & 0 \\ 0 & 0 & 0 \\ 0 & 0 & 0 \end{bmatrix} \psi_{Ra} \tag{16}$$

Equation (16) gives the rate of change in axial displacement for changes in $\tilde{k}_u$.

Figure 32(b) shows the change in lateral displacement as $\tilde{k}_w$ is changed. We obtain this curve by letting $\tilde{k}_\phi$ approach infinity. Thus, the diagonal term reduces to $w_J/w_R = 1 + \left(2/\tilde{k}_w\right)$. The rate of change as $\tilde{k}_w$ is varied is

$$\frac{\partial}{\partial \tilde{k}_w}\psi_{Ja} = \begin{bmatrix} 0 & 0 & 0 \\ 0 & -\frac{2}{\tilde{k}_w^2} & \frac{\ell}{\tilde{k}_w^2} \\ 0 & 0 & 0 \end{bmatrix} \psi_{Ra} \tag{17}$$

Figure 32(c) shows the effect of rotational stiffness $\tilde{k}_\phi$ on beam rotational displacement. The rate of change of beam rotation as $\tilde{k}_\phi$ is changed is

$$\frac{\partial}{\partial \tilde{k}_\phi}\psi_{Ja} = \begin{bmatrix} 0 & 0 & 0 \\ 0 & -\frac{3}{2\tilde{k}_\phi^2} & -\frac{\ell}{2\tilde{k}_\phi^2} \\ 0 & 0 & -\frac{1}{2\tilde{k}_\phi^2} \end{bmatrix} \psi_{Ra} \tag{18}$$

Equation (15) is useful for determining if the joint flexibility needs to be modeled in a truss structure. Above certain threshold values of joint stiffness, the joint deformations can be neglected relative to the beam deformations. For values of joint stiffness above these threshold values, only rigid beam-to-beam connections are necessary in the analysis of a truss. Equations (16), (17), and (18) may be used to determine the sensitivity of the beam deformations to perturbations in joint stiffness. These equations are useful for identifying the importance of nonlinearities in joint stiffness. Since equations (15), (16), (17), and (18) were obtained by modeling the beam with a single linear beam element, these equations should be conservative in the sense that actual beams would be even more flexible than those analyzed herein. Thus, if the joint stiffness has a negligible effect when computed from equation (15), it will certainly be negligible for actual beams. The next section describes the effect of random perturbations in joint stiffness for a truss structure.

Sensitivity of truss frequency to perturbations in joint stiffness. The truss structure shown in figure 26 (without any joint mass) has been analyzed with random perturbations in the axial joint stiffness. A value of $\tilde{k}_u = 0.726$ has been used as an average value about which the stiffness was perturbed. From equation (16), the rate of change of the effective beam stiffness with $\tilde{k}_u = 0.726$ is

$$\frac{\partial}{\partial_{\tilde{k}_u}} \frac{u_J}{u_R} = 3.798$$

Thus, the truss response should be quite sensitive to uniform changes in joint stiffness.

The average axial joint stiffness was randomly perturbed by ±50 percent for each of the 32 truss joints. That is,

$$0.363 \leq \tilde{k}_u \leq 1.088$$

For uniform change in axial stiffness, figure 27 indicates that the frequency of the truss will range from 16.9 Hz at $\tilde{k}_u = 0.363$ to 24.8 Hz at $\tilde{k}_u = 1.088$. The frequency of the truss with an average value of joint stiffness of 0.726 is 21.9 Hz. The truss frequency is indeed quite sensitive to uniform changes in joint stiffness about $\tilde{k}_u = 0.726$.

To assess the effect of random changes in joint stiffness, 35 cases were analyzed to determine the frequency of the truss with random perturbations of each of the 32 joints. Figure 33 shows the results for each of the 35 cases. The fundamental truss frequency has a mean value of 21.2 Hz with a standard deviation of 0.81 Hz.

This moderate variation in frequency shows that the global response may be approximated from the average values of joint stiffness. Even with a ±50-percent perturbation in stiffness, the global frequency change is small. Thus, in the analysis of large truss structures, using the average value of joint stiffness may be adequate to predict global structural behavior. This will greatly reduce the analysis and tracking requirements for modeling each joint with differing stiffnesses.

Conclusions

This study reports a straightforward method for testing joints to determine stiffness and damping coefficients of joint analysis models. The focus of this effort was to obtain finite-element joint models which exhibited load-deflection behavior similar to the measured load-deflection behavior of actual joints. Experiments were used to determine stiffness and damping nonlinearities typical of joint hardware. An algorithm for computing coefficients of analytical joint models based on test data was developed which permits analytical models, linear and nonlinear, to be studied such that the load-deflection behavior exhibited in the experiments can be simulated.

Spring, viscous damper, and friction damper elements were formulated and included in an existing finite-element computer code. Beams with joints have been loaded and their transient response simulated with the finite-element program. The effect of linear and nonlinear joint stiffness on the beam vibration frequency and amplitude was then studied. A truss structure with 32 joints has been analyzed to study the effect of joints on global response. Expressions for predicting the sensitivity of beam deformations to changes in joint stiffness have also been derived. In addition, random perturbations have been used to evaluate the effect of changes in joint stiffness on the frequency of a truss bending mode.

Results from the present study indicate joint stiffness nonlinearities produced nonlinear dynamic response in beam and truss structures for certain joint stiffnesses. For constant vibration amplitude, joint stiffness nonlinearities produced a sinusoidal beam and truss response and the frequency of vibration could be simulated with linearized joint stiffness. However, inaccurate amplitudes of vibration were predicted with the linearized analysis. Random perturbations of joint stiffness produced small changes in global frequency, which indicates the average value of joint stiffness may be adequate to predict global structural behavior. Sensitivity analysis of beams with joints has also been used to develop equations that show values of joint stiffness exist above which the joint flexibility can be neglected in truss structure analysis. The relative stiffness of the joints compared with the truss members is a major parameter that determines the need for modeling the joints.

NASA Langley Research Center
Hampton, VA 23665-5225
January 13, 1987

References

1. Campbell, Thomas G.: Hoop/Column Antenna Technology Development Summary. *Large Space Systems Technology—1980, Volume I—Systems Technology,* Frank Kopriver III, compiler, NASA CP-2168, 1981, pp. 357–364.
2. Mikulas, Martin M., Jr.; Croomes, Scott D.; Schneider, William; Bush, Harold G.; Nagy, Kornell; Pelischek, Timothy; Lake, Mark S.; and Wesselski, Clarence: *Space Station Truss Structures and Construction Considerations.* NASA TM-86338, 1985.
3. Ungar, Eric E.: *Energy Dissipation at Structural Joints; Mechanisms and Magnitudes.* FDL-TDR-64-98, U.S. Air Force, Aug. 1964.
4. Crema, Luigi Ralis; Castellani, Antonio; and Nappi, Alfonso: Damping Effects in Joints and Experimental Tests of Riveted Specimens. *Damping Effects in Aerospace Structures,* AGARD-CP-277, Oct. 1979, pp. 12-1–12-17.
5. Ungar, E. E.: The Status of Engineering Knowledge Concerning the Damping of Built-Up Structures. *J. Sound & Vib.*, vol. 26, no. 1, Jan. 8, 1973, pp. 141–154.
6. Beards, C. F.: Damping in Structural Joints. *Shock & Vib. Dig.*, vol. 11, no. 9, Sept. 1979, pp. 35–41.
7. Aubert, Allen C.; Crawley, Edward F.; and O'Donnell, Kevin J.: *Measurement of the Dynamic Properties of Joints in Flexible Space Structures.* SSL 35-83 (Grant NAGW-21), Space Systems Laboratory, Massachusetts Institute of Technology, Sept. 1983.
8. Soni, M. L.; and Agrawal, B. N.: Damping Synthesis for Flexible Space Structures Using Combined Experimental and Analytical Models. *AIAA/ASME/ASCE/AHS 26th Structures, Structural Dynamics and Materials Conference—A Collection of Technical Papers, Part 2,* Apr. 1985, pp. 552–558. (Available as AIAA-85-0779.)
9. O'Donnell, Kevin J.; and Crawley, Edward F.: *Identification of Nonlinear System Parameters in Space Structure Joints Using the Force-State Mapping Technique.* SSL 16-85 (Grant NAGW-21), Space Systems Laboratory, Massachusetts Institute of Technology, July 1985.
10. Craig, R. R., Jr.: A Review of Time-Domain and Frequency-Domain Component Mode Synthesis Method. *Proceedings of the Joint Mechanics Conference on Combined Experimental/Analytical Modeling of Dynamic Structural Systems,* American Society Mechanical Engineers, 1985, pp. 1–30.
11. Hurty, Walter C.: Dynamic Analysis of Structural Systems Using Component Modes. *AIAA J.*, vol. 3, no. 4, Apr. 1965, pp. 678–685.
12. Hurty, Walter C.; Collins, Jon D.; and Hart, Gary C.: Dynamic Analysis of Large Structures by Modal Synthesis Techniques. *Comput. & Struct.*, vol. 1, no. 4, Dec. 1971, pp. 535–563.
13. Craig, Roy R., Jr.; and Bampton, Mervyn C. C.: Coupling of Substructures for Dynamic Analysis. *AIAA J.*, vol. 6, no. 7, July 1968, pp. 1313–1319.
14. Goldman, Robert L.: Vibration Analysis by Dynamic Partitioning. *AIAA J.*, vol. 7, no. 6, June 1969, pp. 1152–1154.
15. Benfield, W. A.; and Hruda, R. F.: Vibration Analysis of Structures by Component Mode Substitution. *AIAA J.*, vol. 9, no. 7, July 1971, pp. 1255–1261.
16. Kuhar, Edward J.; and Stahle, Clyde V.: Dynamic Transformation Method for Modal Synthesis. *AIAA J.*, vol. 12, no. 5, May 1974, pp. 672–678.
17. Dowell, E. H.: Free Vibrations of an Arbitrary Structure in Terms of Component Modes. *Trans. ASME, Ser. E: J. Appl. Mech.*, vol. 39, no. 3, Sept. 1972, pp. 727–732.
18. Dowell, E. H.: Free Vibrations of a Linear Structure With Arbitrary Support Conditions. *Trans. ASME, Ser. E: J. Appl. Mech.*, vol. 38, no. 3, Sept. 1971, pp. 595–600.
19. Klein, L. R.; and Dowell, E. H.: Analysis of Modal Damping by Component Modes Method Using Lagrange Multipliers. *Trans. ASME, Ser. E: J. Appl. Mech.*, vol. 41, no. 2, June 1974, pp. 527–528.
20. Dowell, E. H.: Component Mode Analysis of Nonlinear and Nonconservative Systems. *J. Appl. Mech.*, vol. 47, no. 1, Mar. 1980, pp. 172–176.
21. Lazan, Benjamin J.: *Damping of Materials and Members in Structural Mechanics.* Pergamon Press, c.1968.
22. Vanderplaats, G. N.: *ADS—A FORTRAN Program for Automated Design Synthesis—Version 1.00.* NASA CR-172460, 1984.
23. Dompka, Robert V.: *Improved Analytic Simulation of Impact Dynamics.* M.S. Thesis, George Washington Univ., Feb. 3, 1984.
24. Noor, Ahmed K.; and Peters, Jeanne M.: Penalty Finite Element Models for Nonlinear Dynamic Analysis. *AIAA/ASME/ASCE/AHS 26th Structures, Structural Dynamics and Materials Conference—A Collection of Technical Papers, Part 2,* Apr. 1985, pp. 369–378. (Available as AIAA-85-0728.)
25. Reissner, Eric: On One-Dimensional Finite-Strain Beam Theory: The Plane Problem. *Z. Angew. Math. & Phys.*, vol. 23, Fasc. 5, Sept. 25, 1972, pp. 795–804.

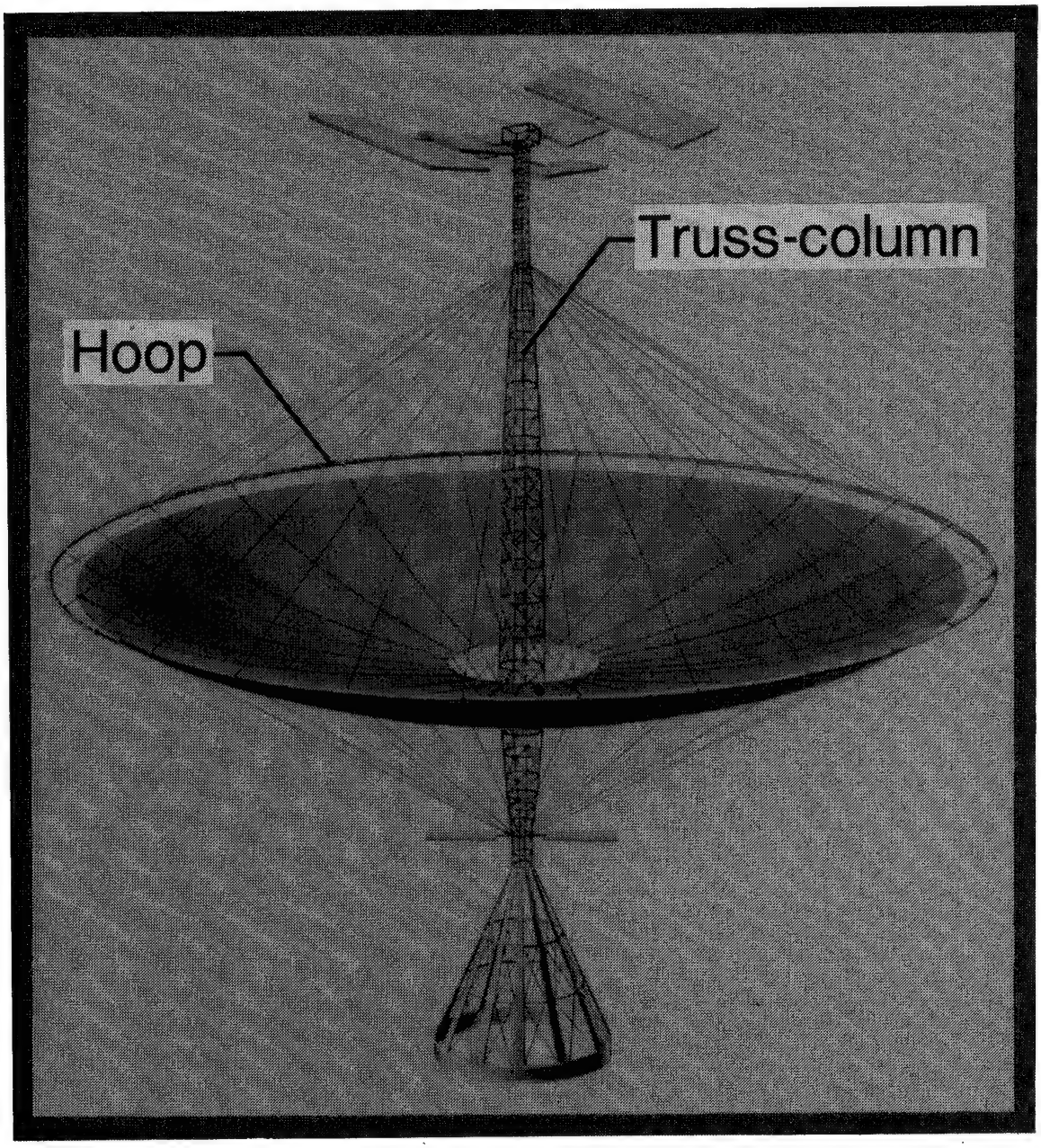

Figure 1. Hoop-column antenna.

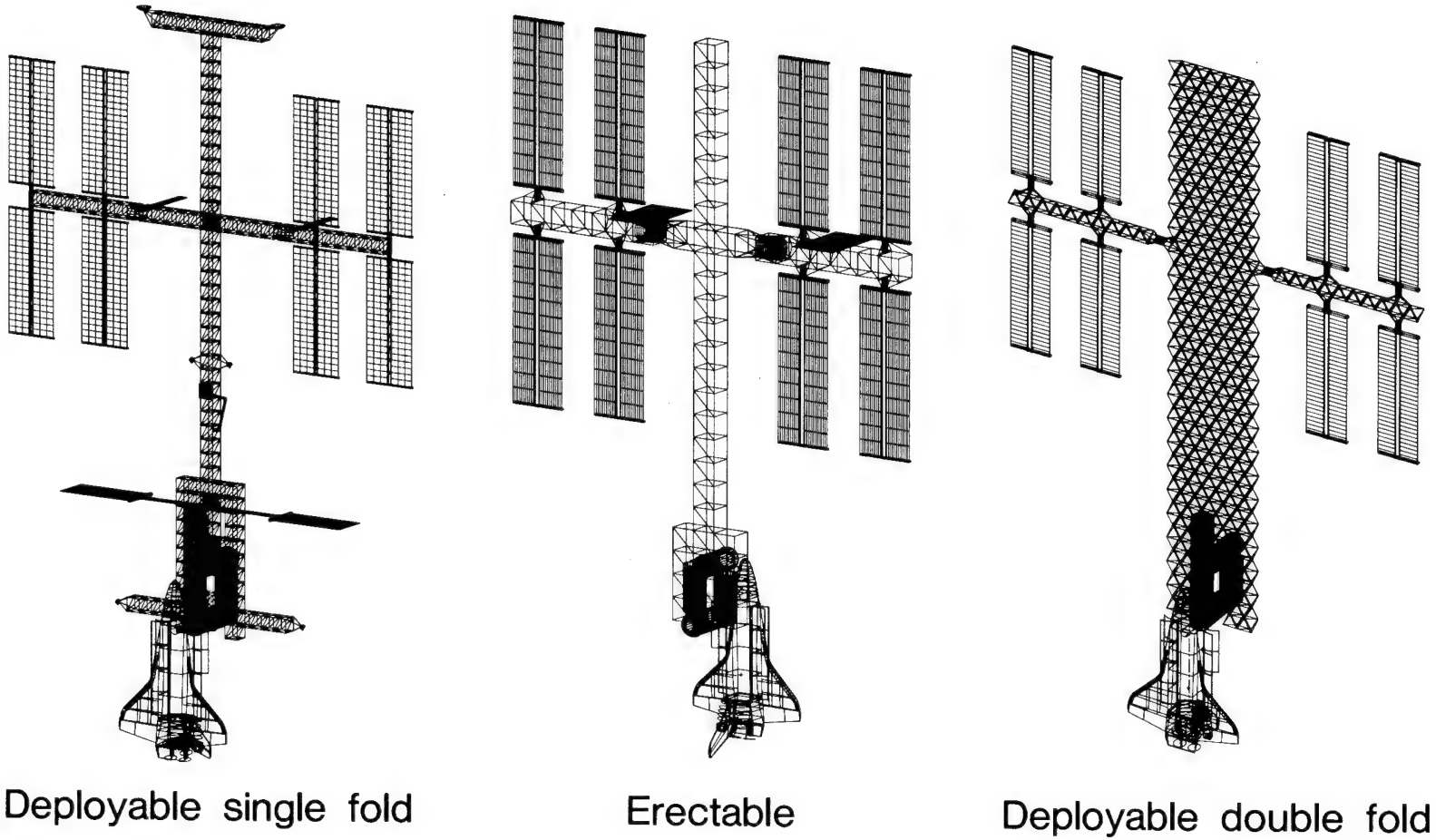

Figure 2. Proposed Space Station configurations.

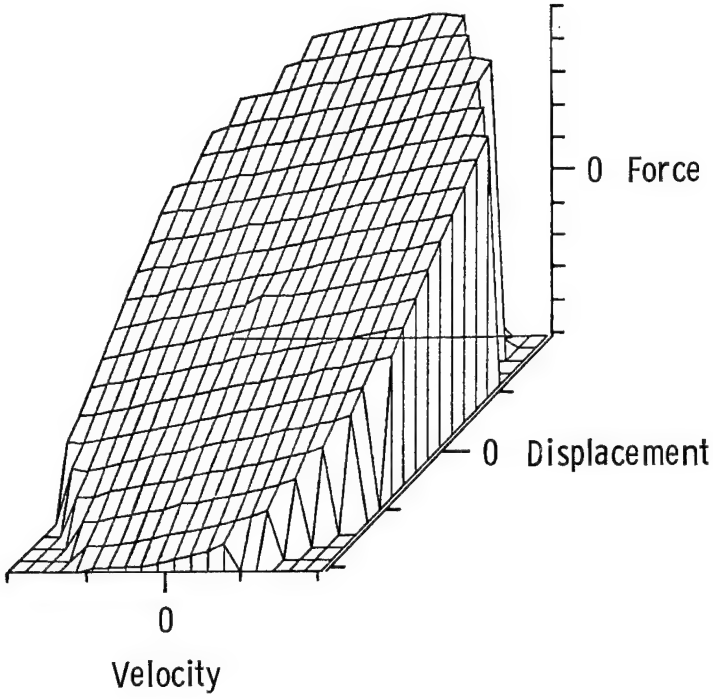

Figure 3. Example of a force-state map.

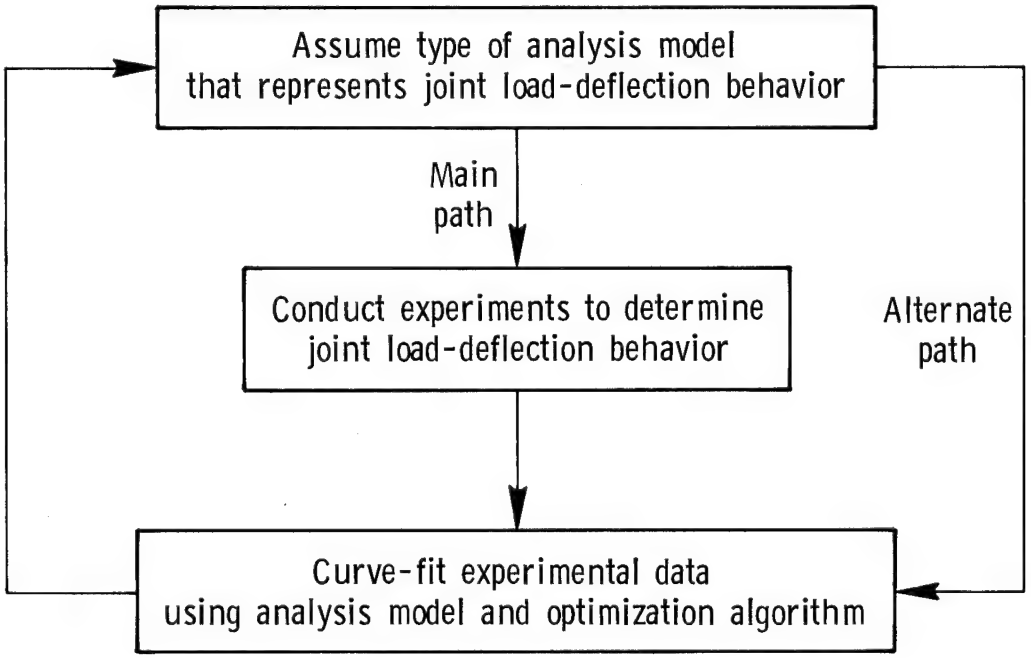

Figure 4. Flowchart for empirical joint model development.

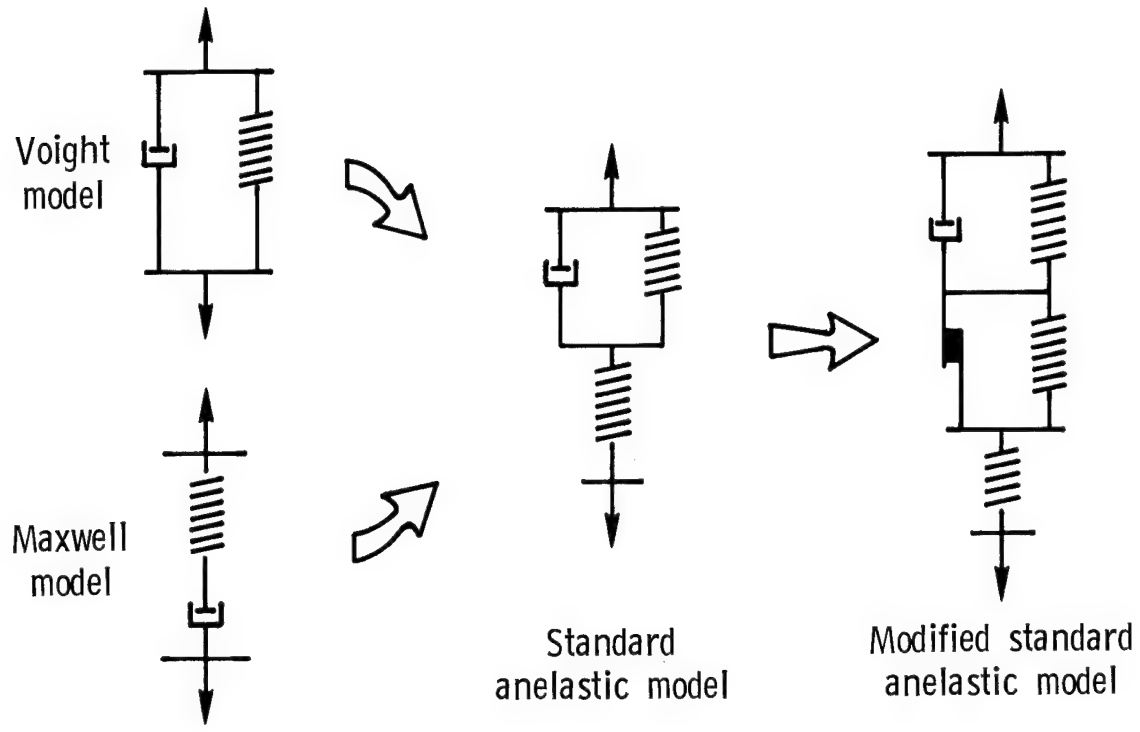

Figure 5. Empirical joint models for material stiffness and damping analysis.

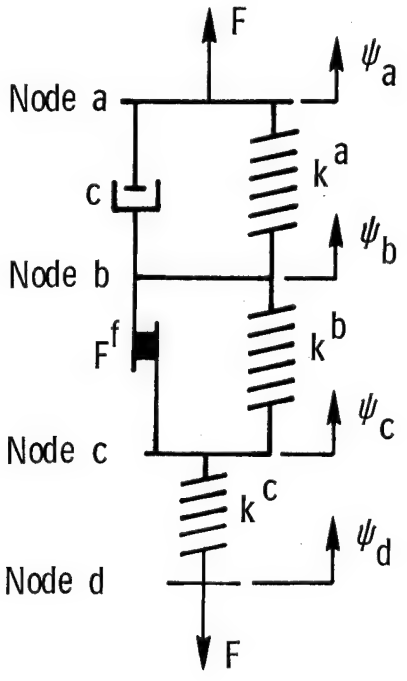

Figure 6. Sign convention for MSA model.

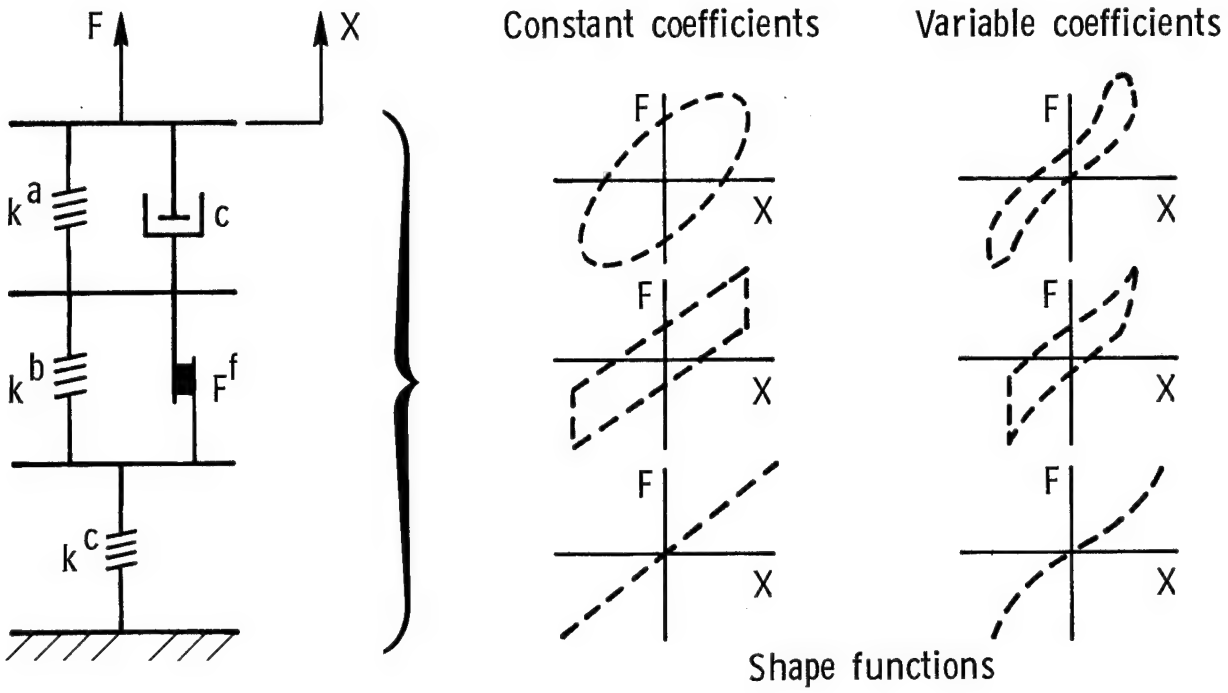

Figure 7. Load-deflection shape functions for constant and variable coefficients.

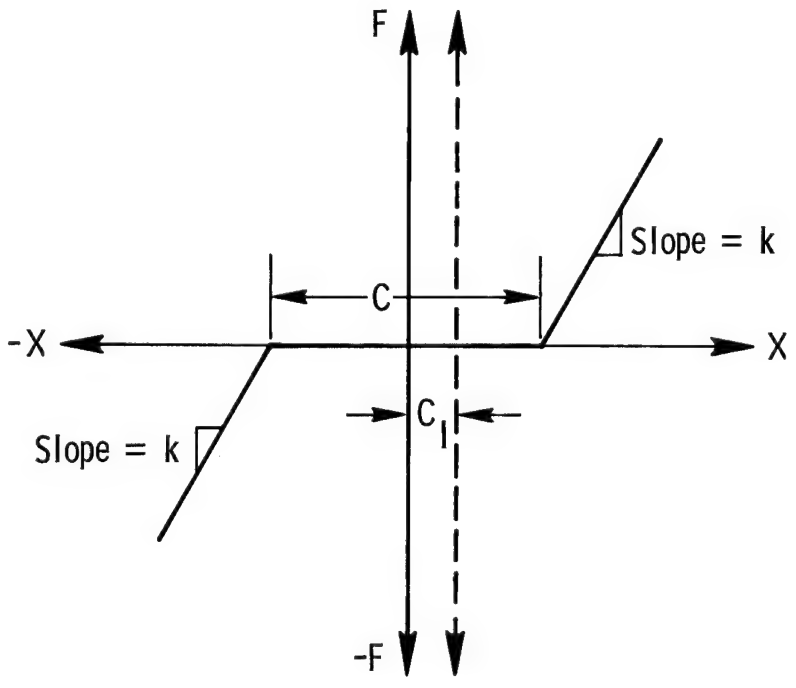

Figure 8. Load-deflection behavior with joint dead band.

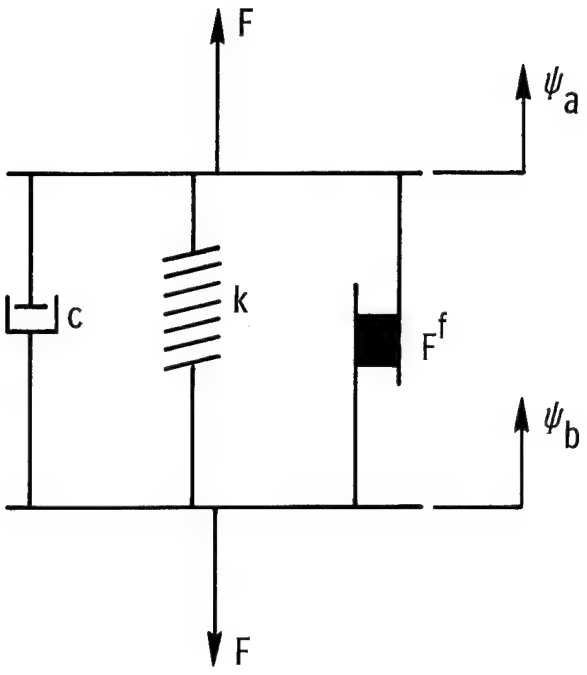

Figure 9. Two-node empirical joint model.

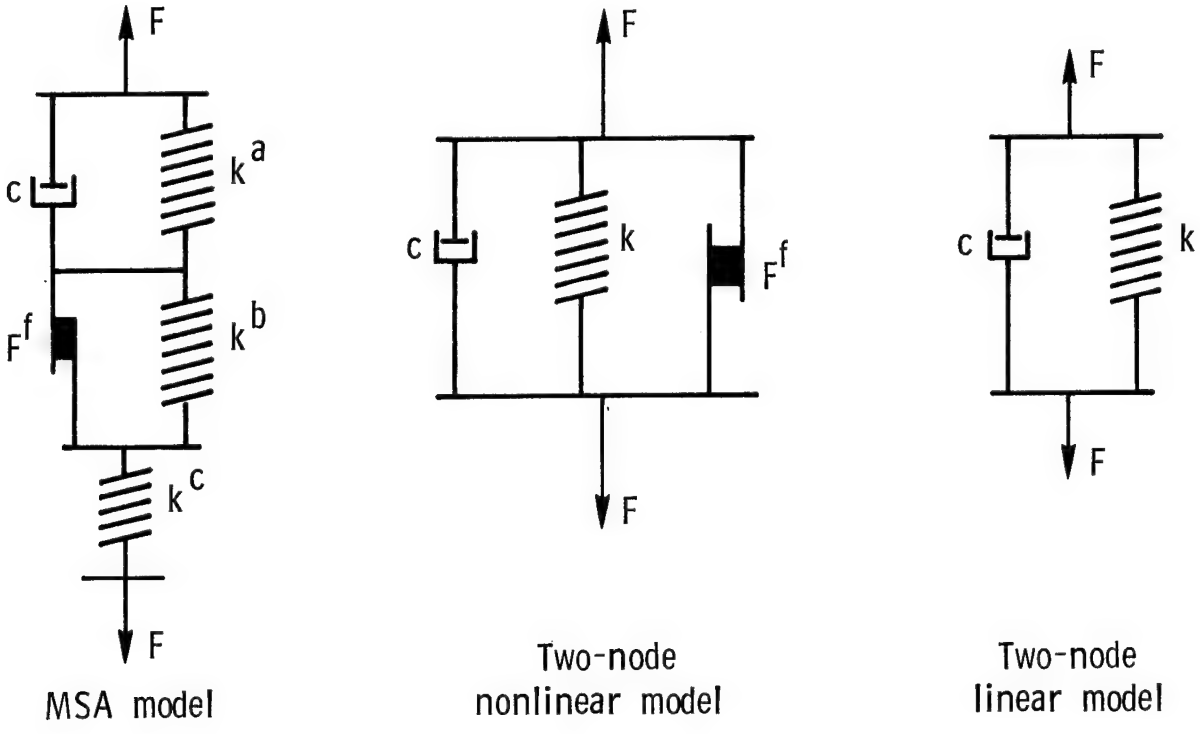

Figure 10. General models for joint simulations.

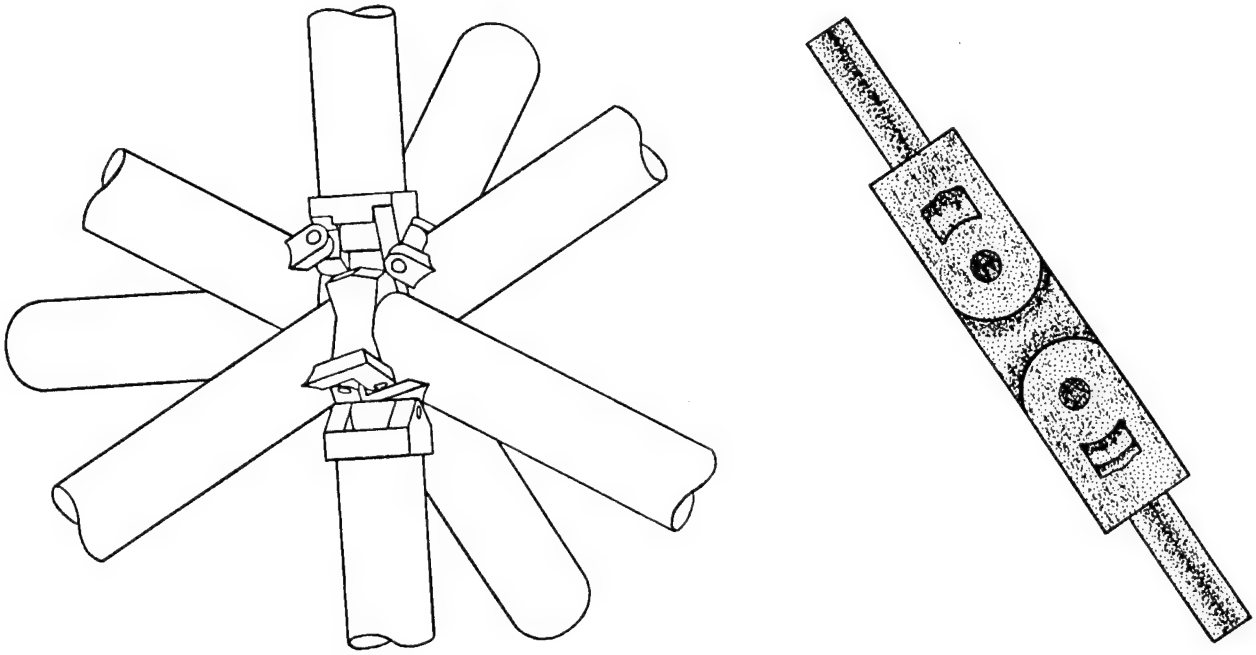

(a) Cluster joint.

(b) Clevis joint.

Figure 11. Typical truss joints for space applications.

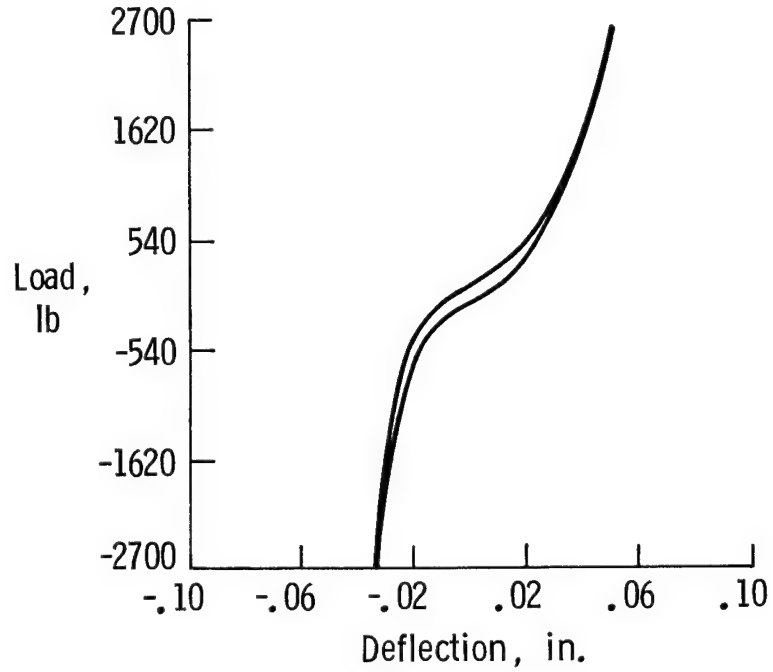

Figure 12. Joint load-deflection test data measured at frequency of 1 Hz.

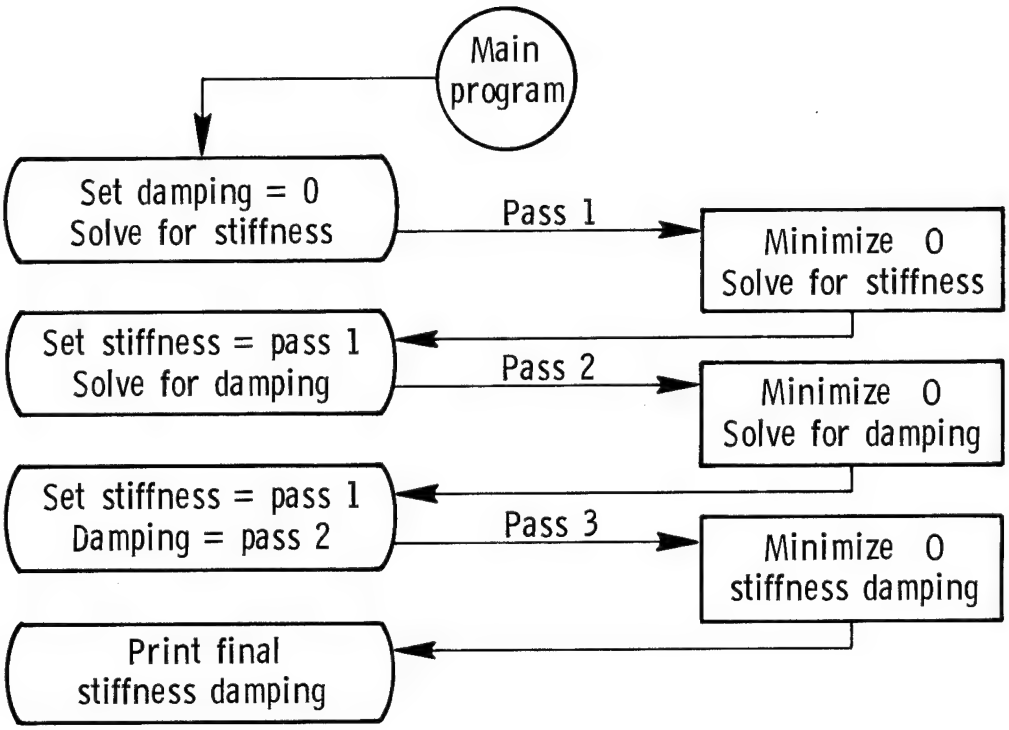

Figure 13. Three-pass solution strategy used in present study.

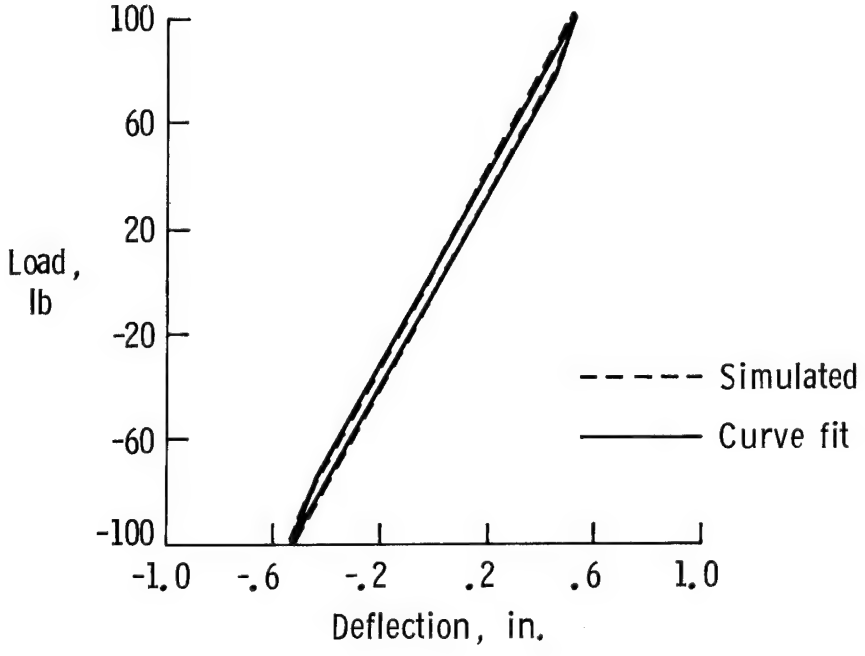

Figure 14. Load-deflection curve fit with simulated data and constant-coefficient MSA model.

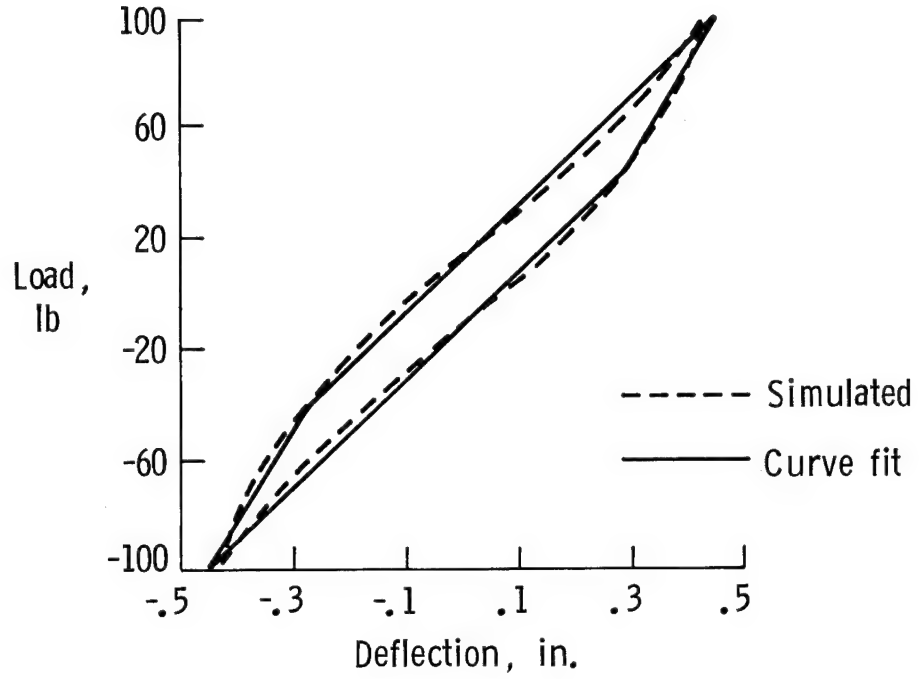

Figure 15. Load-deflection curve fit with nonlinear simulated data and constant-coefficient MSA model.

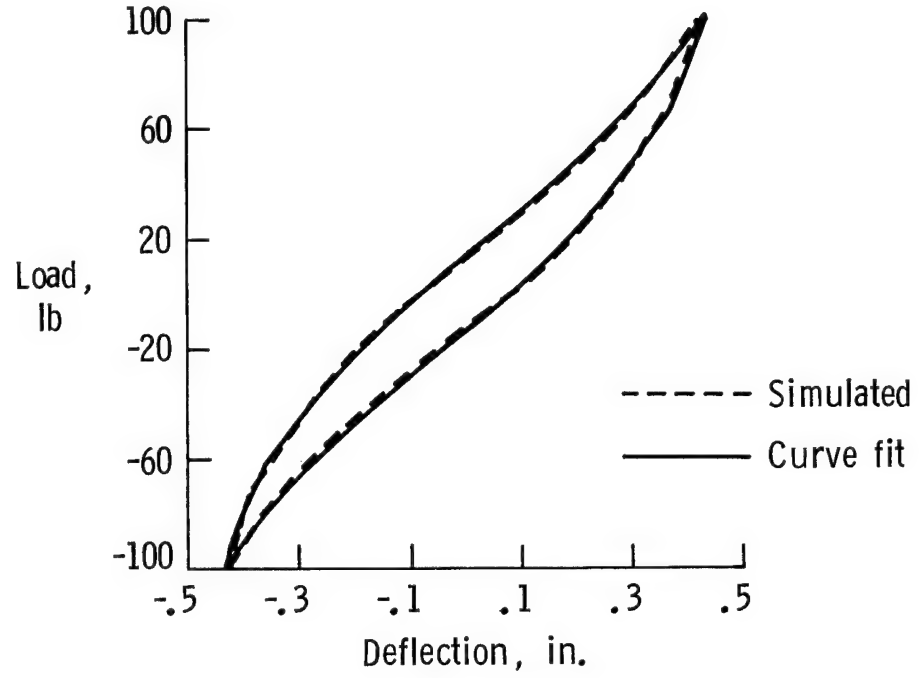

Figure 16. Load-deflection curve fit with nonlinear simulated data and variable-coefficient MSA model.

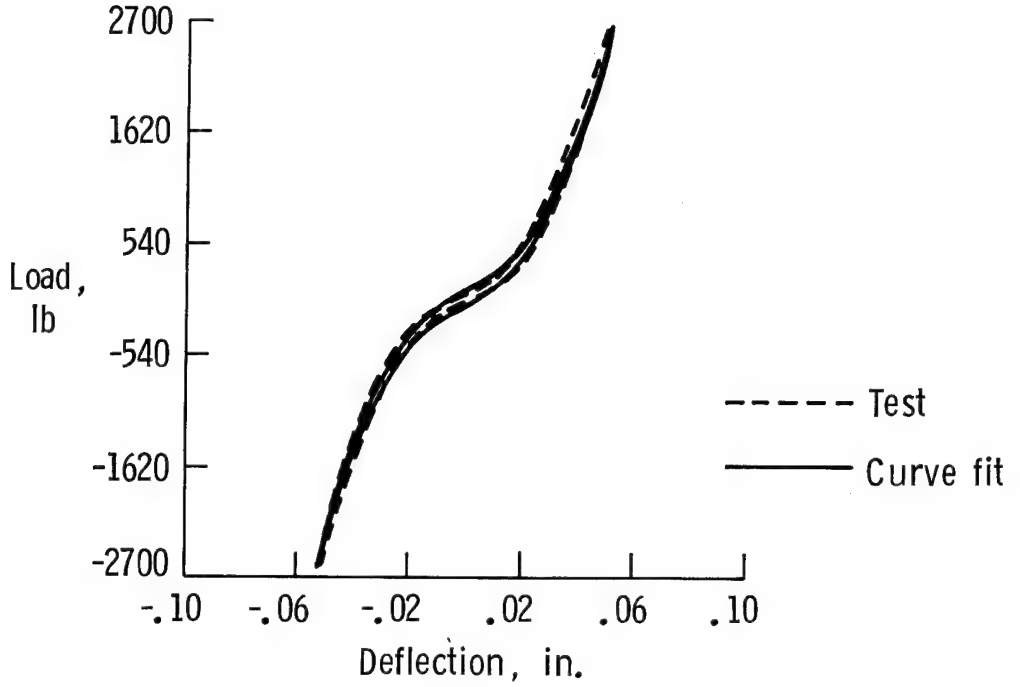

Figure 17. Load-deflection curve fit with test data and variable-coefficient MSA model.

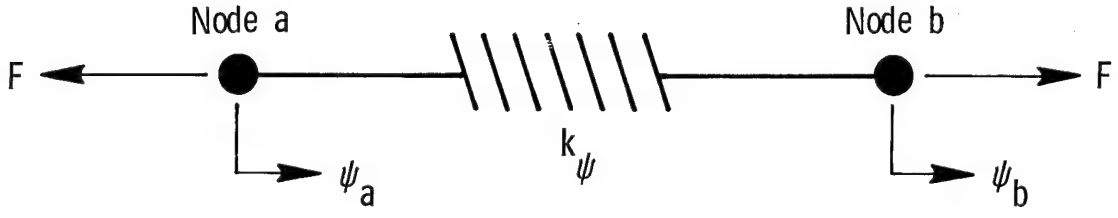

Figure 18. Spring element sign convention.

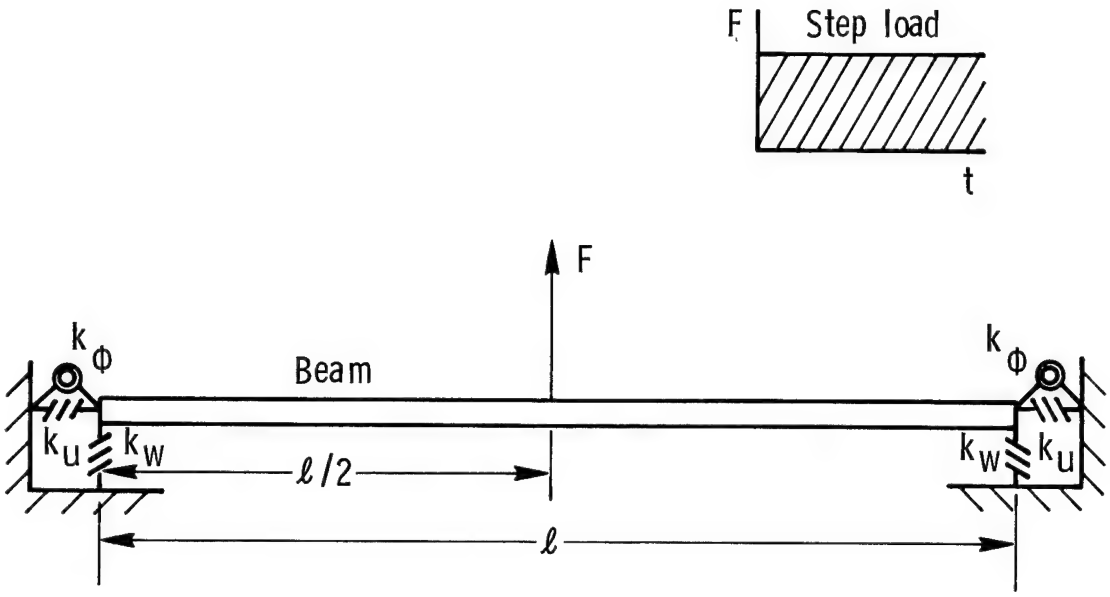

Figure 19. Built-in beam with end joints.

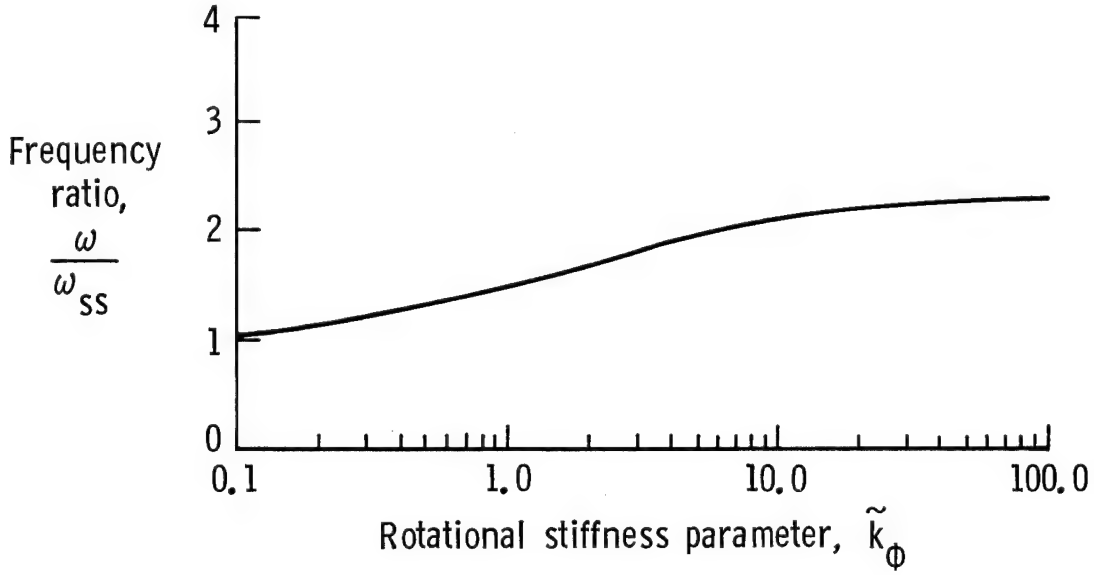

Figure 20. Effect of joint rotational stiffness on beam frequency.

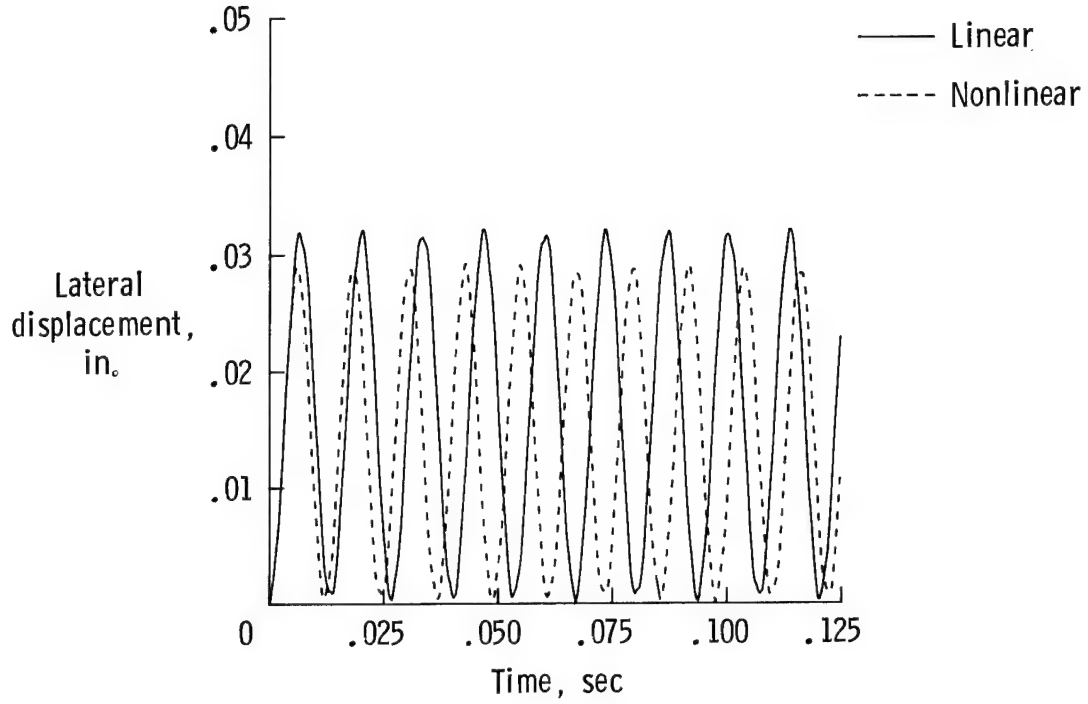

Figure 21. Effect of nonlinear joint stiffness on beam response.

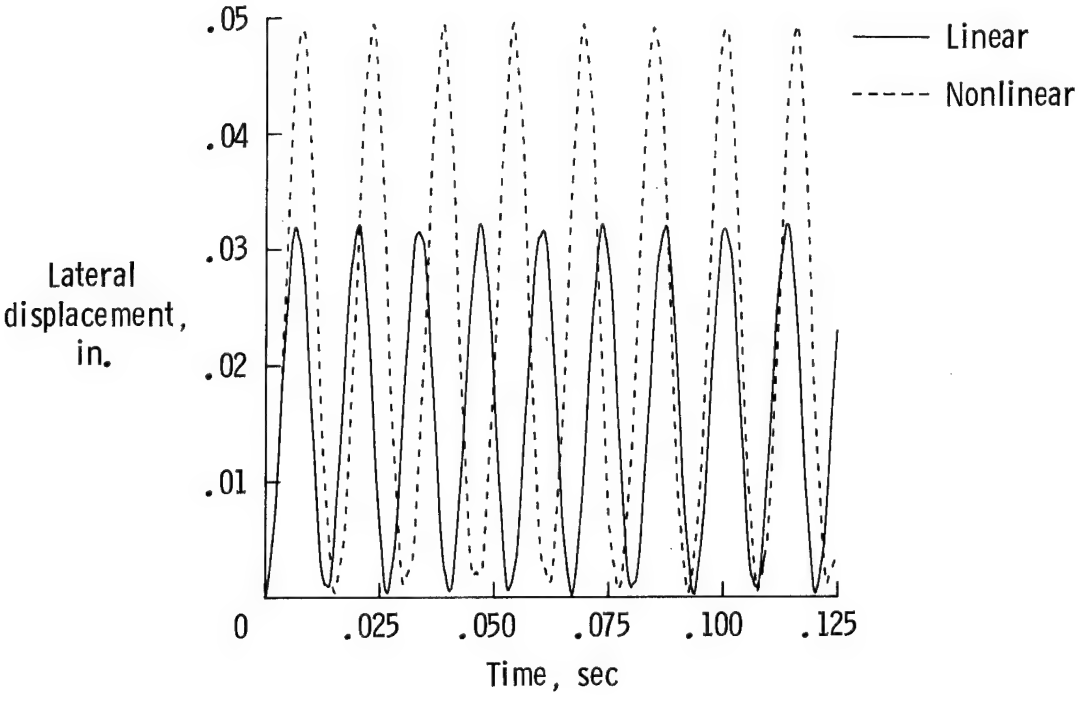

Figure 22. Effect of joint dead band on beam response.

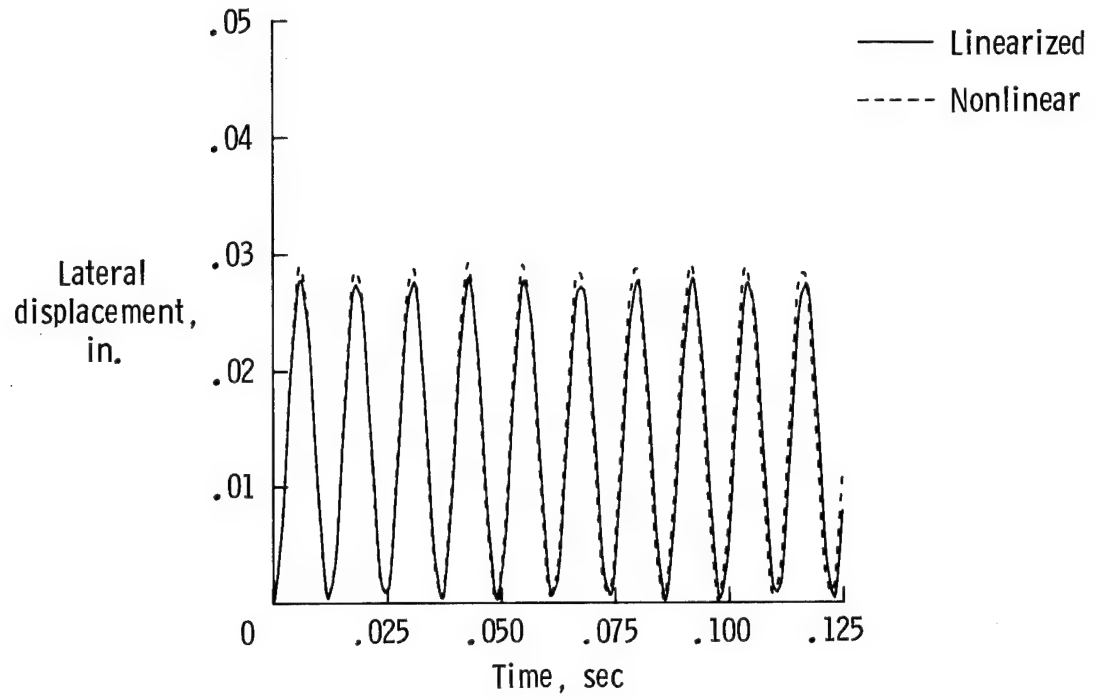

(a) For hardening nonlinearity.

Figure 23. Beam response with linearized joint stiffness.

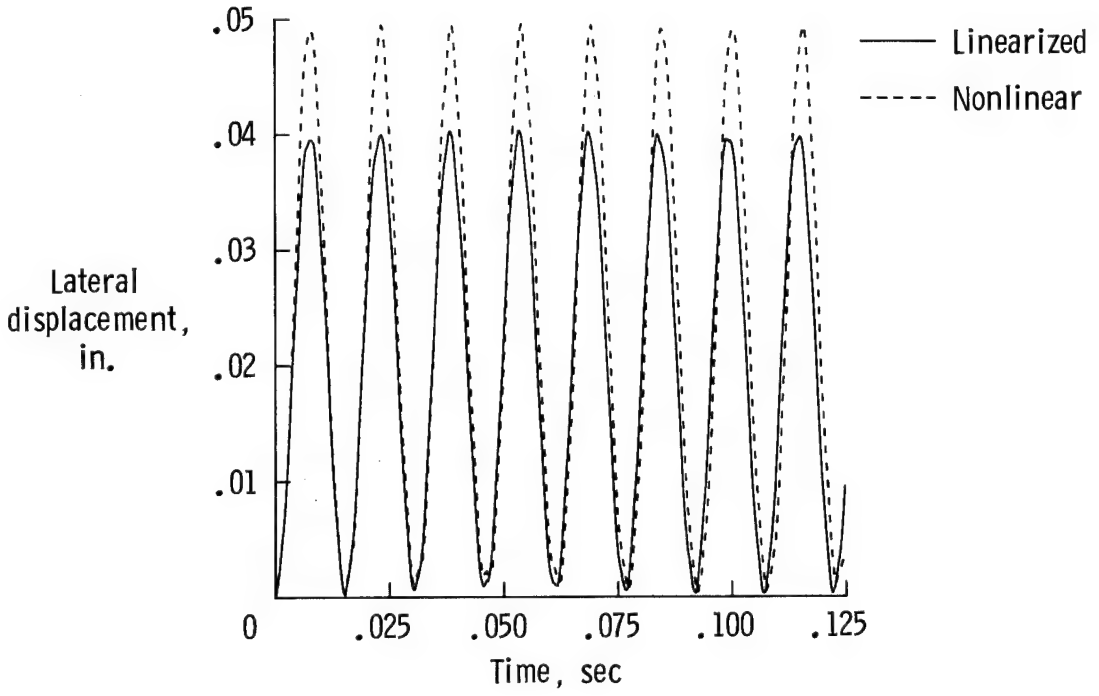

(b) For dead band nonlinearity.

Figure 23. Concluded.

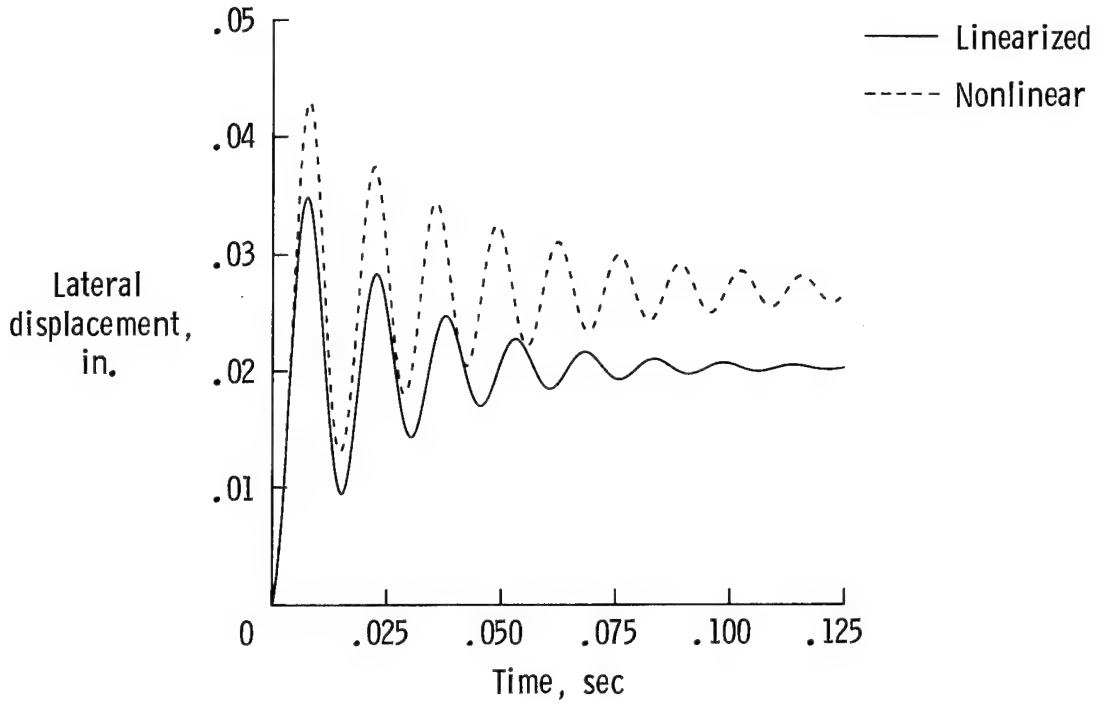

Figure 24. Viscous damped beam response with nonlinear and linearized joint stiffness.

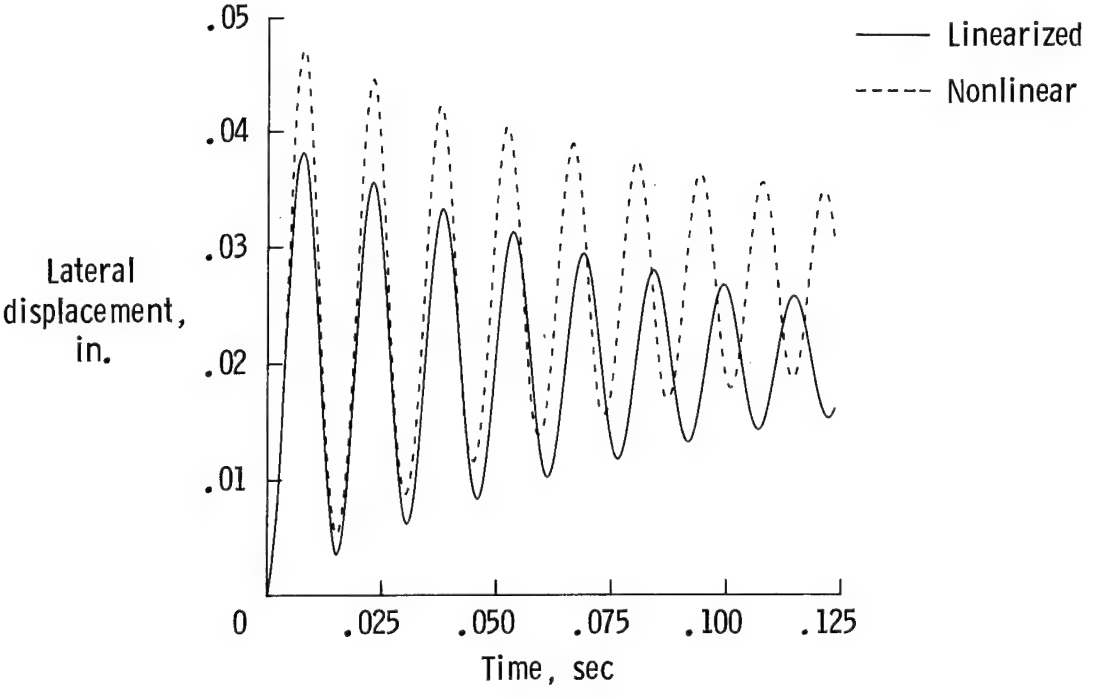

Figure 25. Friction damped beam response with nonlinear and linearized joint stiffness.

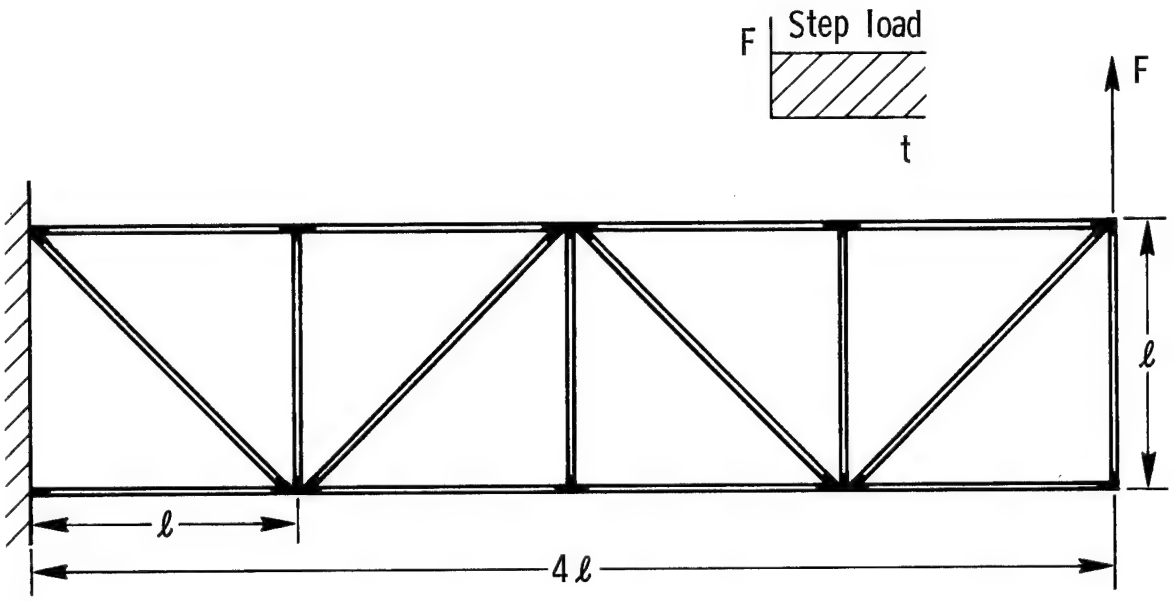

Figure 26. Cantilevered, four-bay truss with joints.

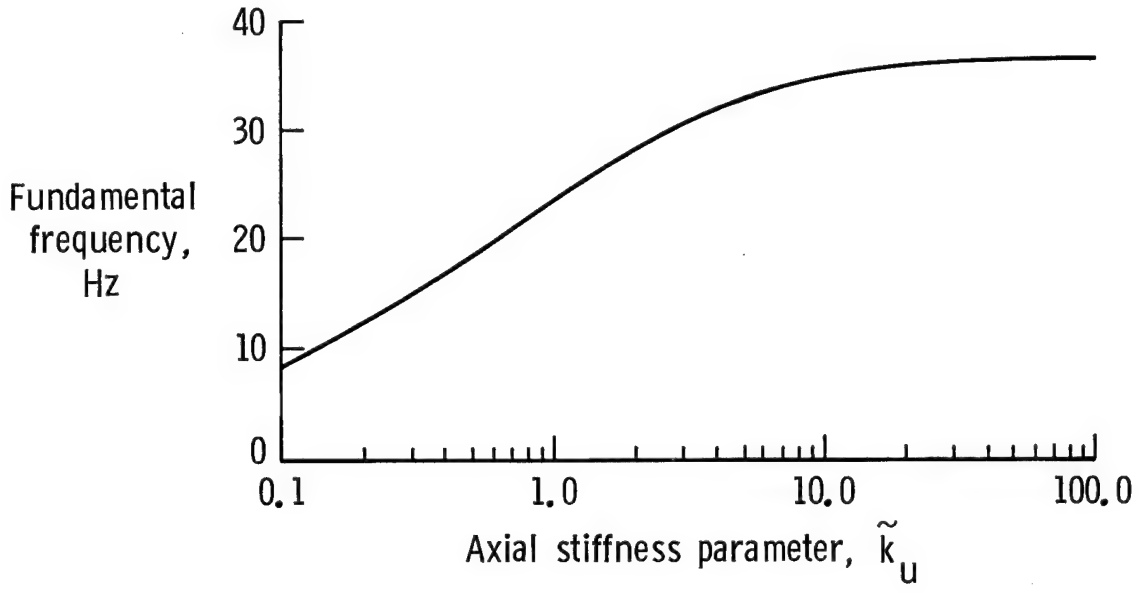

Figure 27. Effect of joint axial stiffness on truss frequency.

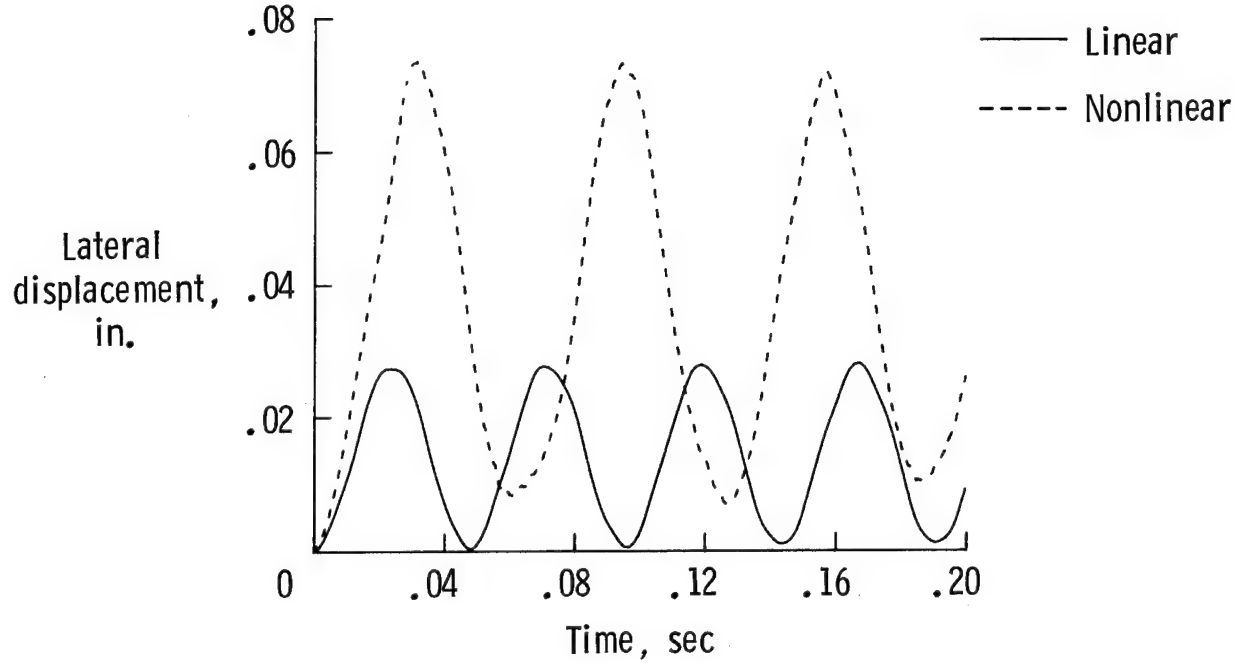

Figure 28. Effect of joint dead band on truss frequency.

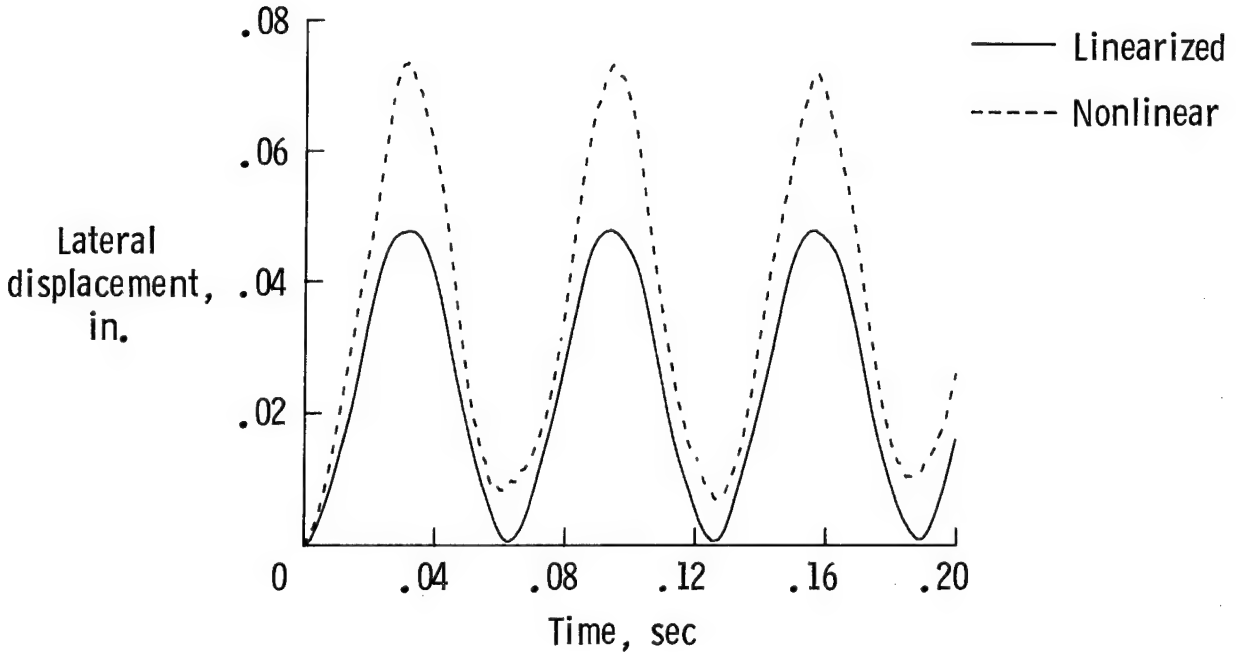

Figure 29. Truss response with linearized joint stiffness for dead band nonlinearity.

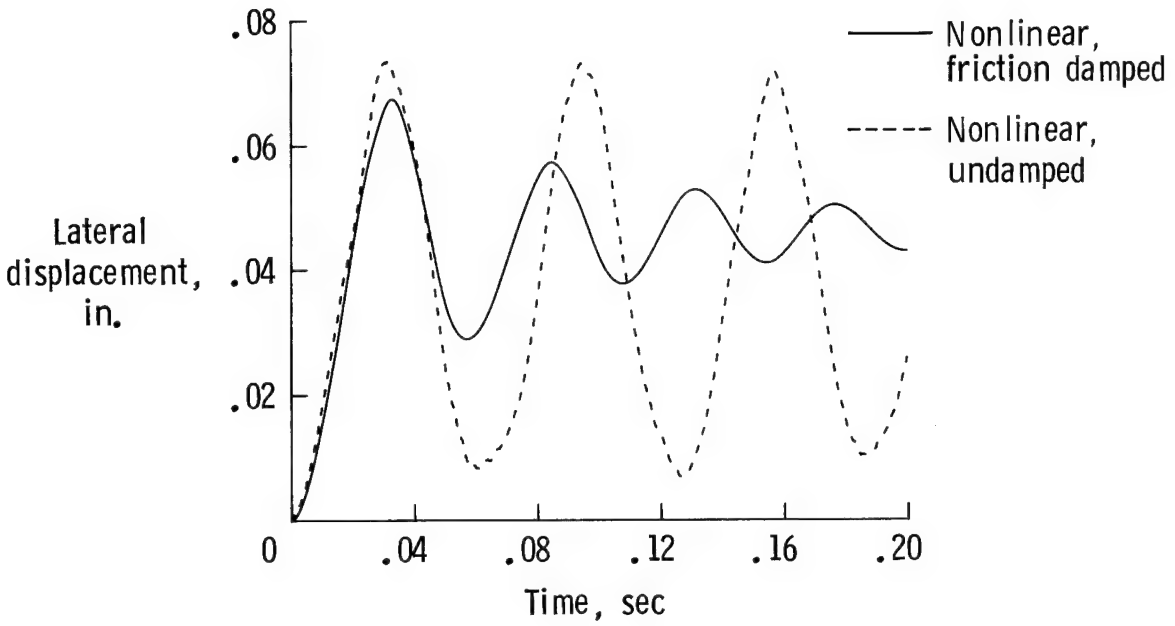

Figure 30. Friction damped truss response with nonlinear joint stiffness.

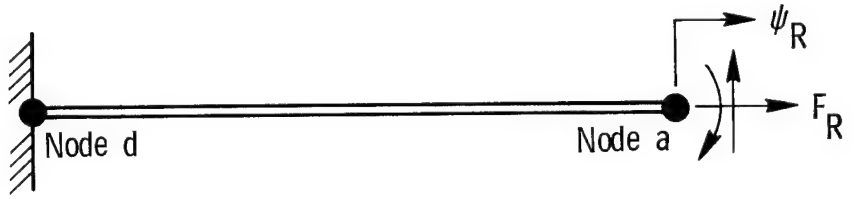

(a) Two-node beam.

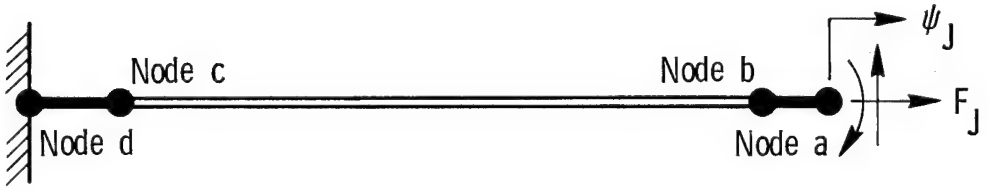

(b) Four-node beam.

Figure 31. Beams used in deformation sensitivity study.

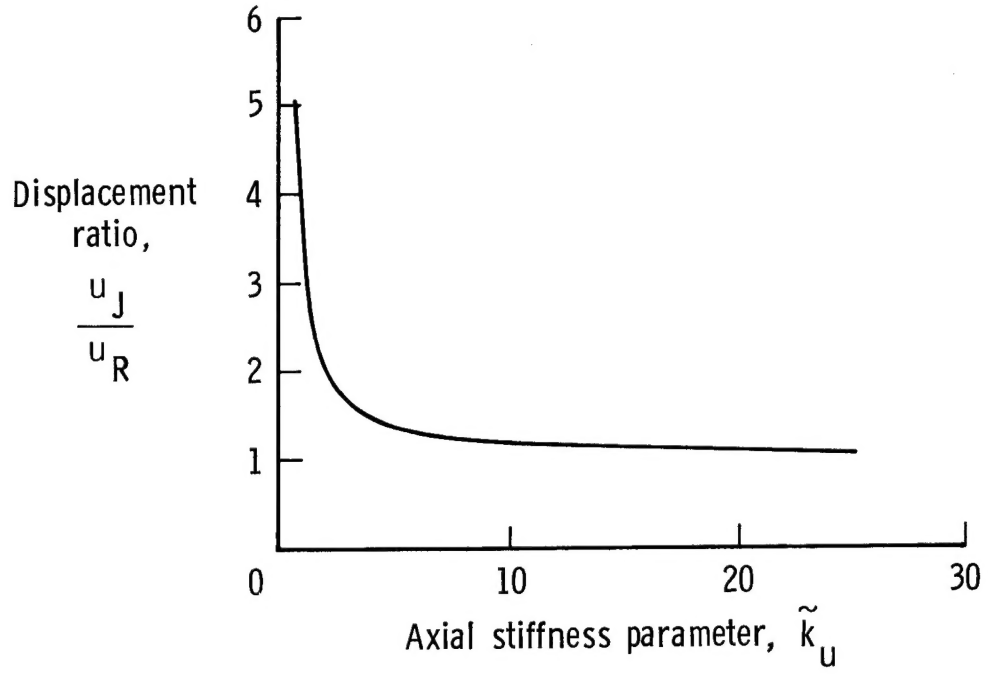

(a) Variation of axial stiffness.

Figure 32. Sensitivity of beam deformations to joint stiffness.

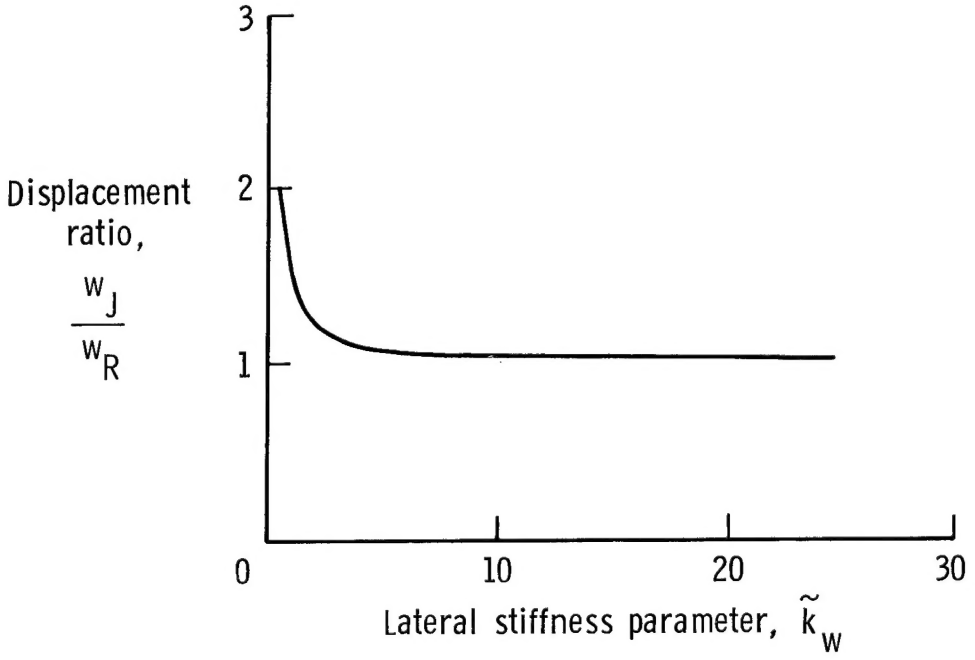

(b) Variation of lateral stiffness.

Figure 32. Continued.

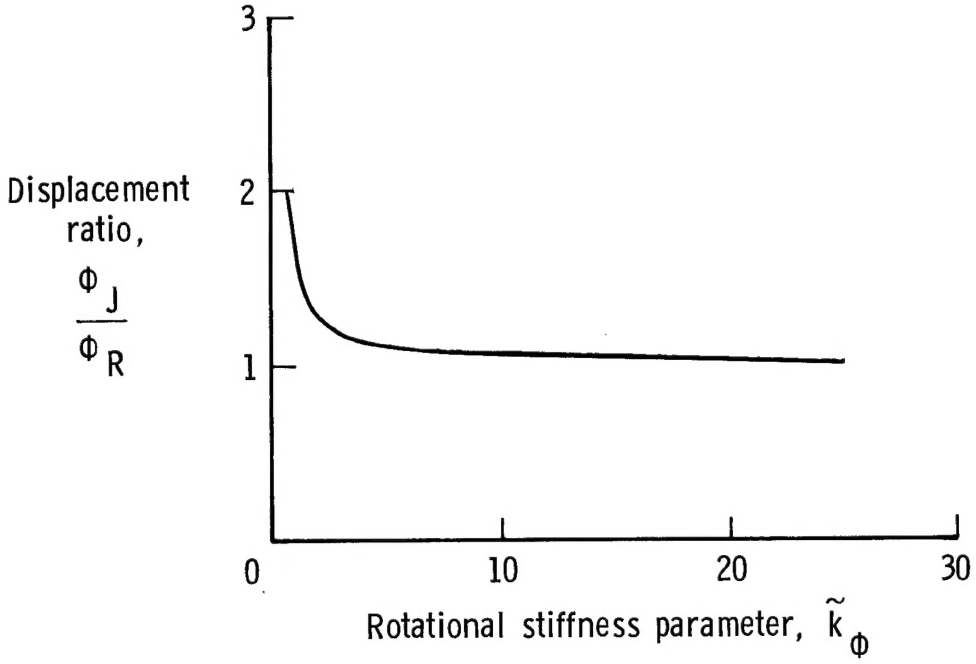

(c) Variation of rotational stiffness.

Figure 32. Concluded.

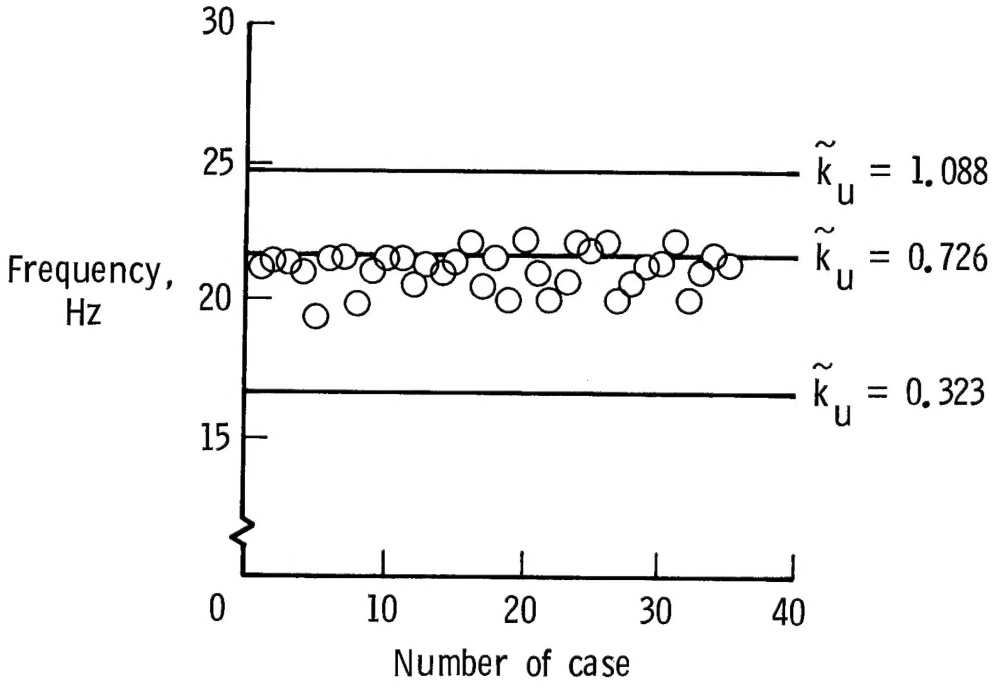

Figure 33. Sensitivity of truss frequency to random perturbations of joint axial stiffness.

Report Documentation Page

1. Report No.	2. Government Accession No.	3. Recipient's Catalog No.
NASA TP-2661		

4. Title and Subtitle	5. Report Date
Modeling of Joints for the Dynamic Analysis of Truss Structures	May 1987
	6. Performing Organization Code

7. Author(s)	8. Performing Organization Report No.
W. Keith Belvin	L-16163

9. Performing Organization Name and Address	10. Work Unit No.
NASA Langley Research Center Hampton, VA 23665-5225	506-43-51-02
	11. Contract or Grant No.

12. Sponsoring Agency Name and Address	13. Type of Report and Period Covered
National Aeronautics and Space Administration Washington, DC 20546-0001	Technical Paper
	14. Sponsoring Agency Code

15. Supplementary Notes

16. Abstract

An experimentally-based method for determining the stiffness and damping of truss joints is described. The analytical models use springs and both viscous and friction dampers to simulate joint load-deflection behavior. A least-squares algorithm is developed to identify the stiffness and damping coefficients of the analytical joint models from test data. The effects of nonlinear joint stiffness such as joint dead band are also studied. Equations for predicting the sensitivity of beam deformations to changes in joint stiffness are derived and used to show the level of joint stiffness required for nearly rigid joint behavior. Finally, the global frequency sensitivity of a truss structure to random perturbations in joint stiffness is discussed.

17. Key Words (Suggested by Authors(s))	18. Distribution Statement
Joints Truss structures Joint-dominated structures Modeling Large space structures	Unclassified—Unlimited Subject Category 39

19. Security Classif.(of this report)	20. Security Classif.(of this page)	21. No. of Pages	22. Price
Unclassified	Unclassified	41	A03

NASA FORM 1626 OCT 86 NASA-Langley, 1987

For sale by the National Technical Information Service, Springfield, Virginia 22161-2171